Agricultural and Forest Meteorology 250–251 (2018) 226–242

Contents lists available at ScienceDirect

Agricultural and Forest Meteorology

journal homepage: www.elsevier.com/locate/agrformet

The risk of tardive frost damage in French vineyards in a changing climate

Giovanni Sgubin[a,*], Didier Swingedouw[a], Gildas Dayon[b], Iñaki García de Cortázar-Atauri[c], Nathalie Ollat[d], Christian Pagé[b], Cornelis van Leeuwen[d]

[a] Environnements et Paléoenvironnements Océaniques et Continentaux (EPOC) – Universitè de Bordeaux, Pessac, France
[b] Climate Modelling and Global Change Team (CERFACS), Toulouse, France
[c] Institut National de la Recherche Agronomique (INRA), US 1116 AGROCLIM, F-84914 Avignon, France
[d] EGFV, Bordeaux Sciences Agro, Universitè de Bordeaux, 33883 Villenave d'Ornon, France

ARTICLE INFO

Keywords:
Climate change
Vitis vinifera L.
General circulation model
Statistical downscaling
Phenological model
Spring frost

ABSTRACT

Tardive frosts, *i.e.* frost events occurring after grapevine budburst, are a significant risk for viticultural practices, which have recently caused substantial yield losses over different winegrowing regions of France, *e.g.* in 2016 and 2017. So far, it is unclear whether the frequency of late frosts events is destined to increase or decrease under future climatic conditions. Here, we assess the risk of tardive frosts for the French vineyards throughout the 21st century by analyzing temperature projections from eight climate models and their statistical regional downscaling. Our approach consists in comparing the statistical occurrences of the last frost (day of the year) and the characteristic budburst date for nine grapevine varieties as simulated by three different phenological models. Climate models qualitatively agree in projecting a gradual increase in temperature all over the France, which generally produces both an earlier characteristic last frost day and an earlier characteristic budburst date. However, the latter notably depends on the specific phenological model, implying a large uncertainty in assessing the risk exposure. Overall, we identified Alsace, Burgundy and Champagne as the most vulnerable regions, where the probability of tardive frost is projected to significantly increase throughout the 21st century for two out of three phenological models. The third phenological model produces opposite results, but the comparison between simulated budburst dates and observed records over the last 60 years suggests its lower reliability. Nevertheless, for a more trustworthy risk assessment, the validity of the budburst models should be accurately tested also for warmer climate conditions, in order to narrow down the associated large uncertainty.

1. Introduction

The development of the grapevine (*Vitis vinifera* L.) follows three main phenological stages, *i.e.* budburst, flowering, veraison, whose timing can significantly determine both the yield and the quality of the crop. The achievement of each phenological stage is predominantly a temperature-driven process (Jones and Davis, 2000; van Leeuwen et al., 2008; Parker et al., 2011, 2013), and the on-going climate change (IPCC, 2013) is currently accelerating all the developmental stages of grapevine in most of the winemaking regions of the globe (Jones et al., 2005; Mira de Orduña 2010; Webb et al., 2011). Future projections suggest that the global warming trend will continue throughout the 21st century (IPCC, 2013), thus potentially further anticipating grapevine phenological phases (Webb et al., 2007; Fraga et al., 2016). Concerning French vineyards, Duchêne et al. (2010) showed that by the end of the 21st century phenological stages in Alsace may advance from by 8–11 days for budburst and up to 16–24 days for veraison of Riesling and Gewurztraminer varieties. Xu et al. (2012) estimated that within the next 30 years flowering and veraison dates may respectively occur 8 and 12 days earlier than present for Pinot noir in Burgundy. Cuccia et al. (2014) assessed that climate conditions 3–5 °C warmer than present may advance the characteristic date of veraison by 3–5 weeks for Pinot noir in Burgundy, while a similar precocity was found for the typical varieties of southern France under an increase of 2–4 °C (Lebon, 2002). In general, the contraction of each phenological phase may yield a precocity of the harvest over France, whose characteristic dates at the end of the 21st century may fall up to 40 days earlier than the current ones (Pieri, 2010; Ollat and Touzard, 2014).

The grapevine budburst process is mainly regulated by the temperature (Garcia de Cortazar-Atauri et al., 2009). Bud development is preceded by a "rest" phase, called endodormancy, during which vegetative growth is physiologically blocked, and by a "quiescence" phase, called ecodormancy, during which unsuitable temperature conditions inhibit the vegetative growth (Sarvas, 1974). Thus, new buds are able

* Corresponding author.
E-mail address: giovanni.sgubin@u-bordeaux.fr (G. Sgubin).

https://doi.org/10.1016/j.agrformet.2017.12.253
Received 15 September 2017; Received in revised form 15 December 2017; Accepted 17 December 2017

to grow after the endodormancy break when environmental conditions become favorable (Chuine, 2000). We classically consider that after a certain exposure to cold temperature (chilling state), the endodormancy status is broken and the action of the accumulated heat (forcing state) starts to be effective for the bud development (Chuine et al., 2003; Garcia de Cortazar-Atauri et al., 2009). Then, after a certain exposure to warm temperatures, this phase culminates with the budburst. Budburst is therefore a key stage for grapevine as it marks the beginning of the growth cycle after dormancy, thus influencing the overall yield and the timing of subsequent phenological stages. In the northern hemisphere, depending on the grape variety and on the local climate, buds commonly break between late winter and early spring. In this phase, the new growing shoots, characterized by high water content, become much more susceptible to freezing temperature than during the winter (Trought et al., 1999). Therefore, an anticipated budburst due to the expected global warming raises the issue of *tardive frosts*, *i.e.* cold events occurring after bud break. A premature budburst may indeed increase the risk to expose the growing tissues to critical cold temperature under which the young shoots may be destroyed. The critical temperature at which a chill injury occurs depends on the growing stage reached as well as on the type of cold event, *i.e.* hoar frost, black frost or freeze (Perry, 1998; Poling, 2008). During budburst, a temperature of −2.2 °C is considered to be lethal for 50% of the buds (Perry, 1998), although temperature around 0 °C can already kill young grape tissues (Trought et al., 1999; Poling, 2008).

A comprehensive analysis of the risks of future tardive frosts in France is missing so far. In particular, it is unclear whether the date of the last frost, which is also expected to recoil under global warming, will advance more than the date of budburst, *i.e.* whether the possibility of damage induced by tardive chill will increase or decrease in the future. Previous studies in other winemaking regions show contrasting results. White et al. (2006) envisaged a general decrease of late frost risks over the United States of America, while Poling (2008) assessed an increased risk in its eastern and mid-west regions. Molitor and Junk (2011) found a widening time gap between the mean last frost and budburst over the last decades in Luxemburg, thus suggesting that the risk of late frost damage has recently decreased under the influence of global warming. It has also been shown that such a local trend is to likely continue for future projections (Molitor et al., 2014). On the contrary, Orlandini et al. (2009) reported that the future earlier budburst is expected to increase the odds of tardive chill in Tuscany (Italy). Also, Mosedale et al. (2015) estimated an increased frequency of late frost events for future projections over the south-west of England. However, these results can be strongly sensitive to the choice of the phenological model for the budburst (Mosedale et al., 2015).

The present work aims at assessing the potential risk of tardive frosts for future climate conditions over France by means of a set of 8 global climate models' projections downscaled at the regional scale. Results are based on a statistical comparison between future trends in budburst and last frost timing. In particular, budburst dates have been calculated by adopting three different phenological models based on the temperature evolution provided by climate model simulations. Overall, our results reveal the qualitative possibility for tardive frost events to increase in the future, notably in the continental regions of France, while in coastal regions this risk is estimated to remain very low or to vanish throughout the 21st century. However, we also show that our assessment strongly depends on the choice of the budburst model, and, to a lesser extent, on the climate model considered.

2. Methods and material

To estimate the risk of tardive frosts in future projections at regional scale, we calculated (*i*) the budburst day and (*ii*) the date of last frost for each single year of climate model projections over France. The method for their calculation can be divided into three main steps:

- Simulation of future climate by means of 8 ocean-atmosphere general circulation climate models (GCM) under RCP8.5 scenario, *i.e.* ACCESS1-3, bcc-csm1-1-m, CanESM2, BNU-ESM, CSIRO-Mk3-6-0, IPSL-CM5A-MR, MIROC5, Nor-ESM1-M.
- Downscaling of the GCM outputs over France.
- Coupling of the downscaled air temperature data with phenological models for budburst stage.

All these procedures imply the use of different climatic and phenological datasets.

2.1. Climate data

For the scope of the present work, we used both past climate data and future projections. Global and regional historical data were necessary to identify statistical relationship for the downscaling process (Section 2.2). For the large scale, we used European Center for Medium-Range Weather Forecast (ECMWF) reanalysis (ERA-Interim) data (Dee et al., 2011), which cover the period from 1979 to present.

We also used higher resolution data from the Safran analysis (Quintana-Segui, 2008; Vidal et al., 2010), which are based on surface observations collected by Météo-France over the period 1959–2015. This dataset consists in hourly and daily temperature data projected on an 8 × 8 km regular grid over France computed through an optimal interpolation algorithm. Safran data have been also used to validate the budburst phenological models (Section 2.3).

Climatic projections are based on simulations of 8 climate models participating to the fifth Coupled Model Intercomparison Project (CMIP5), which provide daily data from 1979 to 2100. Model simulations take into account different emission scenarios from 2006 to 2100, *i.e.* RCP scenarios (Meinshausen et al., 2011), and include a common historical period. However, CMIP5 models run at coarse spatial resolution (around 100 km), which does not allow solving important subgrid scale processes such as those associated with the orography (typically at a scale of a few kilometers).

2.2. Statistical downscaling data

Low-resolution CMIP5 outputs have been projected on a finer grid through statistical downscaling, thus allowing an impact analysis at the regional scale over France. The rationale behind the statistical downscaling stems from the idea that the regional climate depends on the interaction between large-scale meteorological state and local features. Methods of statistical downscaling (see Goodess et al., 2009; Maraun et al. 2010 for a review) consist in establishing an empirical statistical relationship between large-scale variables (predictors) and regional scale variables (predictants) from a set of observational data over a common period called training period. Once the statistical relationships have been established for this period, these can be transferred over a different period and for a different set of low-resolution data, *e.g.* CMIP5 projections as in this study. Thus, statistical downscaling assumes the temporal transferability of the observed statistical relation.

Here we used the *analog* method (Lorenz, 1969), which consists in a re-sampling of the observed atmospheric states. In its formulation proposed by Dayon et al. (2015), statistical relationships between predictors and predictants have been built by comparing low-resolution ERA-Interim data and regional scale Safran data. According to this method, the combination of 7 predictors (sea-level pressure, surface air temperature, air temperature at 500 hPa and 850 hPa, dew point temperature at 850 hPa, specific humidity at 850 hPa and module of moisture flux at 850 hPa) enables to estimate the 2 m air temperature (predictant) over France at finer spatial scale, *i.e.* at a resolution of 8 km for a total of 9892 grid points.

The analog method has the main advantage of maintaining the inter-variable and spatial consistency. Yet, this method may be limited by its inability to reproduce atmospheric states that have not been

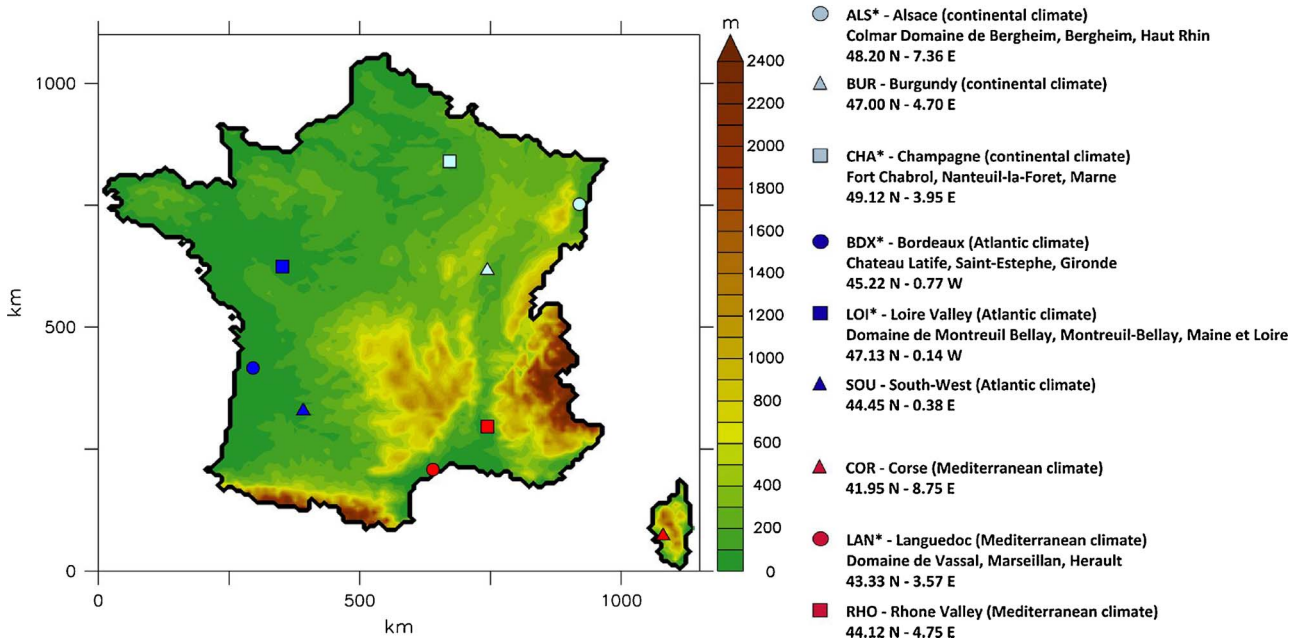

Fig. 1. Map of the altitudes of France (in *m*) and the nine check-points we used in our analysis. Light blue points indicate regions characterized by a continental climate (Alsace, Burgundy and Champagne), dark blue points indicate regions characterized by the Atlantic climate (Bordeaux, Loire Valley and South-West), while the red points indicate the region characterized by a Mediterranean climate (Corse, Languedoc and Rhone Valley). The stars in the legend indicate locations where historical observations of the budburst day were available. (For interpretation of the references to colour in this figure legend, the reader is referred to the web version of this article.)

observed during the training period.

2.3. Budburst observed data

Observed budburst dates have been used for testing the validity of the different phenological models. We based such validation on the PHENOCLIM database (https://w3.avignon.inra.fr/perpheclim/), which regroups the phenological data of the main traditional varieties collected by the French National Agronomic Research Institute (INRA) throughout the last decades (Quintana-Segui, 2008). These observations include five different vineyard regions and capture the main climatic diversity over France, *i.e.* Champagne and Alsace for the continental climate (*cf.* Fig. 1), Loire Valley and Bordeaux for the Atlantic climate, and Languedoc for the Mediterranean climate. The five stations are located in Nanteuil-la-Forêt (Champagne), Bergheim (Alsace), Montreuil-Bellay (Loire Valley), Saint-Estèphe (Bordeaux) and Marseillan (Languedoc) as detailed in Fig. 1. Four supplementary checkpoints have been also added in order to extensively cover the main French vineyards for the analysis of the risk of tardive frost, *i.e.* Burgundy, Corse, Rhone Valley and South-West region (Fig. 1). The budburst records cover the period between 1959 and 2002 with a number of samples that varies from region to region. The main observed budburst dates for different grapevine varieties in the five checkpoints are reported in Table 1. The PHENOCLIM database was also at the base of the calibration of two of the budburst models we adopted in this work (Garcia de Cortazar-Atauri et al., 2009).

2.4. Phenological model for the budburst

Downscaled temperature data over France have been successively used to force a phenological model calculating the date of budburst for the 9 most representative grapevine varieties in France, *i.e. Chardonnay*, *Riesling*, *Sauvignon blanc* and *Ugni blanc* for the white varieties, and *Cabernet-Sauvignon*, *Grenache*, *Merlot*, *Pinot noir* and *Syrah* for the red varieties. These varieties can be classified in relation to their heat requirement for bud break, from early budding varieties like Chardonnay, Pinot noir and Riesling, to late budding varieties like Cabernet-Sauvignon, Grenache and Ugni blanc (van Leeuwen et al., 2008).

Phenological models assume that budburst process is induced by a sequence of certain temperature conditions after the dormancy induction. In general, a budburst model consists in (*i*) a dormancy (cold action) sub-model calculating the chill accumulation required to overcome the endodormancy, and (*ii*) a post-dormancy (warm action) sub-model computing the heat accumulation from the end of endodormancy necessary for the bud break. Thus, the endodormancy break (simply called dormancy break hereinafter) identifies two different periods, namely (*i*) the dormancy period charactering the chilling state, and (*ii*) the post-dormancy period characterizing the forcing state. According to this approach, the dormancy break occurs once a critical chilling C_{crit} has been accumulated starting from the initial day t_0, which ideally represents the beginning of dormancy. For a given year, by considering the daily chilling units C_u, the day of dormancy break t_{db} hence occurs when:

$$\sum_{t_0}^{t_{db}} C_u \approx C_{crit} \tag{1}$$

In turn, the budburst coincides with the fulfillment of a critical temperature forcing F_{crit} formalized in terms of the cumulative daily forcing units F_u after the day of dormancy break t_{db}. For a given year, the date of budburst t_{bb} hence occurs when:

$$\sum_{t_{db}}^{t_{bb}} F_u \approx F_{crit} \tag{2}$$

The critical thresholds F_{crit} and C_{crit} are based on optimization calculation and depend on the different grapevine cultivars. Depending on the different formulations of the chilling and forcing actions, various budburst models have been developed. In the present study, we adopted three different phenological models, *i.e.* (*i*) a simple thermal time growing degree-day model (GDD model) in which the dormancy break is not calculated but predefined by fixing a constant starting date for the forcing units accumulation, (*ii*) a sequential phenological model (BRIN model) in which the dormancy break, calculated using a constant threshold C_{crit}, is followed by a post-dormancy period whose length is calculated using constant a threshold F_{crit} and (*iii*) a parallel phenological model (the FENOVITIS model), in which the dormancy break is

Table 1
Observed budburst dates in the historical period and performance of the three phenological models computed through the RMSEP of the modeled budburst dates. Observed data are those obtained from the PHENOCLIM database in 5 different locations over France. For each of the 9 varieties considered, the RMSEP is computed by comparing all the available observed budburst dates with the corresponding modeled budburst dates according with the 3 phenological models.

Cepage	Region	Samples	Mean budburst day (DOY)	RMSEP GDD_5	RMSEP BRIN	RMSEP FENOVITIS
Cabernet-Sauvignon	Alsace	28	122 ± 9	9.7	11.1	/
	Bordeaux	8	84 ± 7			
	Languedoc	27	89 ± 7			
	Loire	8	114 ± 10			
Chardonnay	Alsace	28	112 ± 10	15.5	13.1	24.3
	Champagne	5	106 ± 11			
	Languedoc	20	75 ± 9			
Grenache	Alsace	27	118 ± 10	17.5	19.1	/
	Languedoc	24	83 ± 8			
	Loire	5	121 ± 13			
Merlot	Alsace	28	117 ± 10	11.1	10.7	/
	Bordeaux	42	90 ± 16			
	Languedoc	18	78 ± 8			
Pinot noir	Alsace	47	114 ± 8	9.4	7.9	/
	Champagne	5	110 ± 9			
	Languedoc	28	78 ± 8			
Riesling	Alsace	47	115 ± 9	10.8	9.8	/
	Languedoc	12	84 ± 8			
	Loire	6	113 ± 9			
Sauvignon blanc	Alsace	13	111 ± 10	13.4	13.3	/
	Languedoc	40	86 ± 7			
	Loire	5	120 ± 17			
Syrah	Alsace	27	114 ± 10	16.6	17.4	/
	Languedoc	20	79 ± 11			
	Loire	5	111 ± 10			
Ugni blanc	Alsace	27	122 ± 10	7.9	8.2	/
	Loire	5	120 ± 9			

also calculated using a constant C_{crit} but the F_{crit} threshold to calculate the budburst completion depends on the chilling state.

The choice of these specific phenological models is based on an optimized selection for the scope of this study. The GDD_5 and the BRIN models are the most performant in simulating realistic budburst dates over France for present-day conditions, among the different phenological models evaluated by Garcia de Cortazar-Atauri et al. (2009). At the same time, the FENOVITIS-like models (not included in the evaluation of Garcia de Cortazar-Atauri et al., 2009) are the most widely used models when projecting the impacts of future climate change on the budburst of grapevine (Caffarra and Eccel, 2011; Molitor et al., 2014; Mosedale et al., 2015). Moreover, the comparison between a thermal time model (GDD_5), a sequential model (BRIN) and a parallel model (FENOVITIS) allows for a detailed assessment of the potential uncertainty associated with the different typologies of models. Further details concerning the formulation of the three phenological models and their key references are provided in Appendix A.

2.5. Statistical assessment for future late frost risks

Along with the estimation of t_{bb} by means of a phenological model, for each year we also calculated the day of the last frost t_{lf}, defined as the last day of the year before summer for which the surface temperature satisfies certain critical conditions. The risk of frost damage depends on both duration and intensity of cold temperatures to which the grapevine is exposed. Here, we set two critical limits to define a frost day, *i.e.* $Tavg < 2\,^{\circ}C$, which guarantees a certain duration of daily cold temperatures (as in Mosedale et al., 2015) and $T_{min} < -2\,^{\circ}C$, which guarantees a certain severity of night frost. Hereinafter, we will refer to as frost day that day satisfying such conditions. Nevertheless, sensitivity tests using different definitions for frost days have been also performed and discussed.

To evaluate the possibility of tardive chill over a given period of N years, we compared the statistical features associated with t_{bb} with the statistical features associated with t_{lf}. Both t_{bb} and t_{lf} are stochastic variables, which can be characterized by their different probability density functions $p_{bb}(t)$ and $p_{lf}(t)$, describing the likelihood for a generic day *t* of the year to be respectively a day of budburst and a day of last frost for a given period of N years. We assumed a Gaussian distribution for t_{bb}. Thus, once calculated the mean day of occurrence m_{bb} (which represents the characteristic date of occurrence over a period of N years) and the associated standard deviation σ_{bb} over a period of N years, its probability density function p_{bb} is:

$$p_{bb}(t) = \frac{1}{\sigma_{bb}\sqrt{2\pi}} e^{-\frac{(t-m_{bb})}{2\sigma_{bb}^2}} \tag{3}$$

By defining t_0 and t_f the extremes of a single year growing season, its cumulative distribution function $P_{bb}(t)$ at the end of the growing cycle, *i.e.* at $t = t_f$, is:

$$P_{bb} = \sum_{t=t_0}^{t_f} p_{bb}(t) = 1 \tag{4}$$

The latter implies that the budburst is an event that surely occurs for each single year of the period considered.

Since the conditions at the base of the definition of last frost day may be not always encountered over a period of N years, we defined N_f as the number of years satisfying such a condition for at least one day over a single year, with $N_f \leq N$. By calculating the mean of the last frost day m_{lf} and the associated standard deviation σ_{lf} for the N_f years featuring at least one frost event, we defined the probability density function p_{lf} by scaling the Gaussian distribution as:

$$p_{lf}(t) = \frac{N_f}{N} \frac{1}{\sigma_{lf}\sqrt{2\pi}} e^{-\frac{(t-m_{lf})}{2\sigma_{lf}^2}} \tag{5}$$

Hence, its cumulative distribution function $P_{lf}(t)$ at the end of the annual growing cycle, *i.e.* at $t = t_f$, is:

$$P_{lf} = \sum_{t=t_0}^{t_f} p_{lf}(t) = \frac{N_f}{N} \tag{6}$$

Thereby, for a given period of N years, by taking into account that

budburst and frost days are independent events, the probability of a tardive frost p_{tf}, *i.e.* the chance that the budburst date t_{bb} occurs at a day $t = t^*$ and that date falls prior to the last frost date, can be formalized as follows:

$$p_{tf}(t^*) = p(t^* = t_{bb} \cap t^* \leq t_{lf}) = p_{bb}(t^*)\left[1 - \sum_{t=t_0}^{t^*} p_{lf}(t)\right] \quad (7)$$

where t_0 has been set to the 1st of October. Hence, by considering all the days of the growing season of a single year, *i.e.* $t \in [t_0, t_f]$ the total probability P_{tf} that the budburst occurs prior to the last frost day is

$$P_{tf} = \sum_{t^*=t_0}^{t_f} \left\{ p_{bb}(t^*)\left[1 - \sum_{t=t_0}^{t^*} p_{lf}(t)\right]\right\} \quad (8)$$

These parameters have been calculated for each single climate model simulation, and our assessment is based on their ensemble mean. An illustrative example of the step-by-step calculation of the modeled present and future probability P_{tf} in three different locations is provided in Appendix B.

3. Calculation

3.1. Evaluation of the downscaling method for future projections

The statistical relationships between large and local scales that are calculated over a historical training period may not necessarily subsist for a different period, notably if global warming is involved. The analog method here adopted, may not be able to correctly project, at regional scales, unprecedented synoptic conditions of the atmosphere, *i.e.* large-scale atmospheric states that have never been registered during the training period. Therefore, in our specific case, one may eventually find a disagreement between downscaled temperature and the main temperature trends and variability produced by the original low-resolution CMIP5 simulations. A common procedure to evaluate the accuracy and the transferability of the downscaling method for future projections is to compare the downscaled predictants, *i.e.* surface air temperature in our case, with that directly produced by the GCM model. Although the analog method was comprehensively validated in Dayon et al. (2015), we further tested the accuracy of the downscaling method over the 9 chosen checkpoints (Fig. 1). To do that, we calculated the correlation between the downscaled temperature and the GCM temperature. We did it for the different seasons, finding statistically significant correlations (95% level) between coarse and downscaled data for all the climate models used here (Table 2), which give confidence in the downscaling method used.

Table 2
Evaluation of the downscaling method across the different climate models, through correlation between downscaled outputs and coarse resolution (original) climate outputs. The evaluation has been performed over the 9 checkpoints illustrated in Fig. 1 and for the different seasons of the year. Values indicate the mean and standard deviations of the correlations *r* among the different checkpoints. All the correlations from the table are statistically significant above the 95% confidence level.

CMIP5 models	r winter	r spring	r summer	r autumn
ACCESS1-3	0.91 ± 0.03	0.95 ± 0.01	0.93 ± 0.04	0.93 ± 0.01
bcc-csm1-1-m	0.90 ± 0.02	0.93 ± 0.01	0.92 ± 0.03	0.92 ± 0.01
BNU-ESM	0.90 ± 0.03	0.94 ± 0.02	0.92 ± 0.03	0.94 ± 0.01
CanESM2	0.89 ± 0.04	0.94 ± 0.01	0.95 ± 0.02	0.91 ± 0.01
CSIRO-Mk3-6-0	0.90 ± 0.02	0.95 ± 0.01	0.94 ± 0.04	0.92 ± 0.01
IPSL-CM5A-MR	0.87 ± 0.03	0.94 ± 0.02	0.92 ± 0.03	0.93 ± 0.01
MIROC5	0.90 ± 0.02	0.94 ± 0.01	0.93 ± 0.03	0.92 ± 0.01
Nor-ESM1-M	0.78 ± 0.04	0.83 ± 0.03	0.73 ± 0.05	0.83 ± 0.02

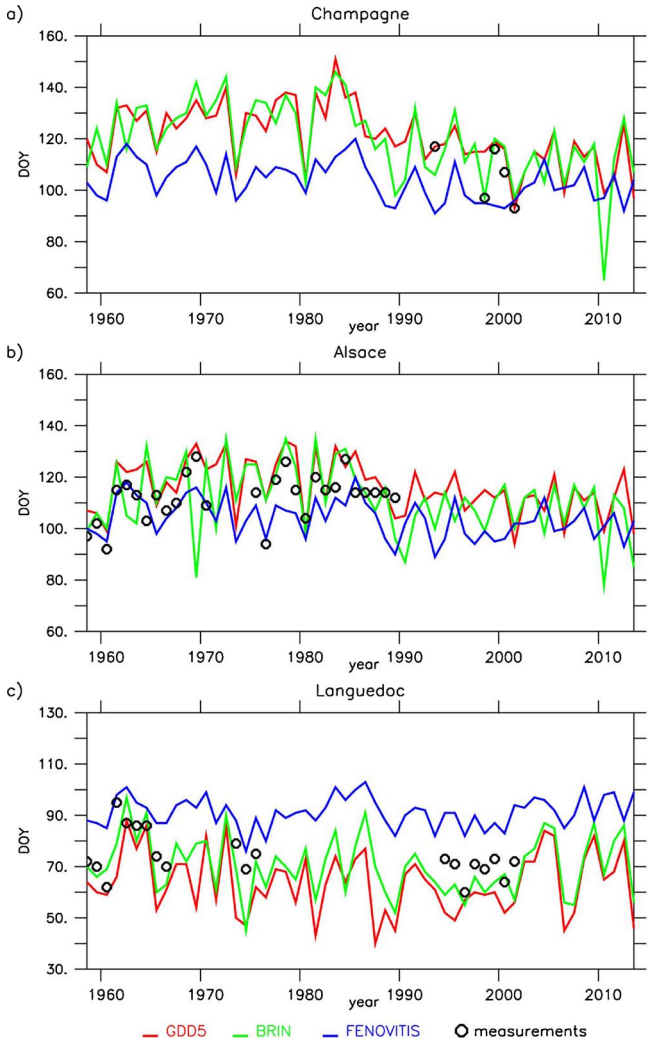

Fig. 2. Time series of the simulated budburst dates calculated using Safran temperature data (in *DOY*) for Chardonnay over (a) Champagne, (b) Alsace and (c) Languedoc. *Red lines* indicate results obtained with GDD_5 model, *green lines* indicate results obtained with BRIN model and *blue lines* indicate results obtained with FENOVITIS model. *Circles* indicate the measured budburst date according with PHENOCLIM dataset. (For interpretation of the references to colour in this figure legend, the reader is referred to the web version of this article.)

3.2. Performance of the phenological models

The historical dates of budburst from various locations, *i.e.* PHENOCLIM dataset, have been used for the validation of the different phenological models. The accuracy of GDD_5, BRIN and FENOVITIS models were evaluated by using the root mean square error of prediction (RMSEP) of their simulated budburst dates computed using Safran data in each location from the corresponding observed data (Table 1). The GDD_5 and the BRIN models show a similar performance, with 9 days < RMSEP < 20 days in accordance with the results from Garcia de Cortazar-Atauri et al. (2009). Compared with the latter, we found here RMSEP values that are, on average, slightly higher. However, in the current analysis, the budburst dates have been calculated over a 64 km^2 region, hence not exactly coinciding with the point where meteorological measurements were made. Errors evidenced by the FENOVITIS for the Chardonnay are greater, *i.e.* RMSEP > 20 days. However, it should be noted that the calibration of this model complies with climatic conditions registered over the northeastern part of Italy, so that it may not necessarily fit with mean climatic conditions over France. An example of the different performances of phenological models is illustrated in Fig. 2, showing the time series of the modeled

Chardonnay budburst dates in three different regions as well as the available corresponding observations. These examples represent well the main characteristics featured by the different models. The GDD_5 and BRIN models appear to plausibly represent the mean budburst date in Champagne and Alsace while they simulate a slightly premature budburst date in Languedoc. The FENOVITIS model simulates a slightly premature budburst over Champagne and Alsace, while it reproduces a more tardive budburst over Languedoc. Also, both GDD_5 and BRIN regions appear to better capture the interannual variability in budburst date, while FENOVITIS seems to underestimate it. These features suggest therefore that FENOVITIS model is less sensitive to differences in temperature, thus implicitly implying that the effects of global warming on the simulation of the budburst day may be underestimated by this model.

4. Results

To investigate the mean temperature changes over France throughout the 21st century and their influence on the potential occurrence of late frosts, we focused on two different periods of 30 years featuring the mean climate (*i*) at the beginning (1980–2009) and (*ii*) at the end (2071–2100) of the CMIP5 simulations.

4.1. Future trends of air temperature over France

In Fig. 3 we show the anomaly of annual air temperature for the projections' ensemble mean between the end of the 21st century (2071–2100) and the baseline period (1980–2009) for each season. The comparison between these periods evidences that the surface air temperature tends to increases everywhere over France for RCP8.5 scenario. However, temperature increases vary both temporally and spatially. The most smoothed signal occurs in winter, when mean temperature anomaly ΔT over France is $2.4 \pm 0.69\,^{\circ}C$ for RCP8.5 scenario. The warming signal amplifies in spring ($\Delta T = 3.6 \pm 0.72\,^{\circ}C$ for RCP8.5) and reaches its peak during summer ($\Delta T = 5.3 \pm 1.52\,^{\circ}C$ for RCP8.5), while autumn evidences the second most moderate warming signal ($\Delta T = 3.1 \pm 0.54\,^{\circ}C$ for RCP8.5).

Furthermore, the warming pattern appears to be amplified in the continental regions of France while it is more moderate in proximity of the coastal regions bordering the Atlantic and the Mediterranean due to inertial effect of the sea on temperature changes.

4.2. Last frost occurrence in future projections

The characteristic day of the year m_{lf} featuring the last frost strongly depends on the region considered (Fig. 4). For the period 1980–2009 it typically varies from end-of-January/beginning-of-February for the Mediterranean sector to end-of-March/beginning-of-April for continental regions (Fig. 4a). In the mountainous regions, *i.e.*, the Alps, the Massif Central and the Pyrenees, it occurs even later, but we do not consider these areas in our analysis. The increase in 2-m air temperature over France under future climate scenarios provokes an overall anticipation of the characteristic last frost day m_{lf}. For the period 2071–2100 it occurs, on average, around 20 days earlier than currently, with anomalies generally higher in the western part of France than in the eastern part (Fig. 4b). However, such an assessment does not

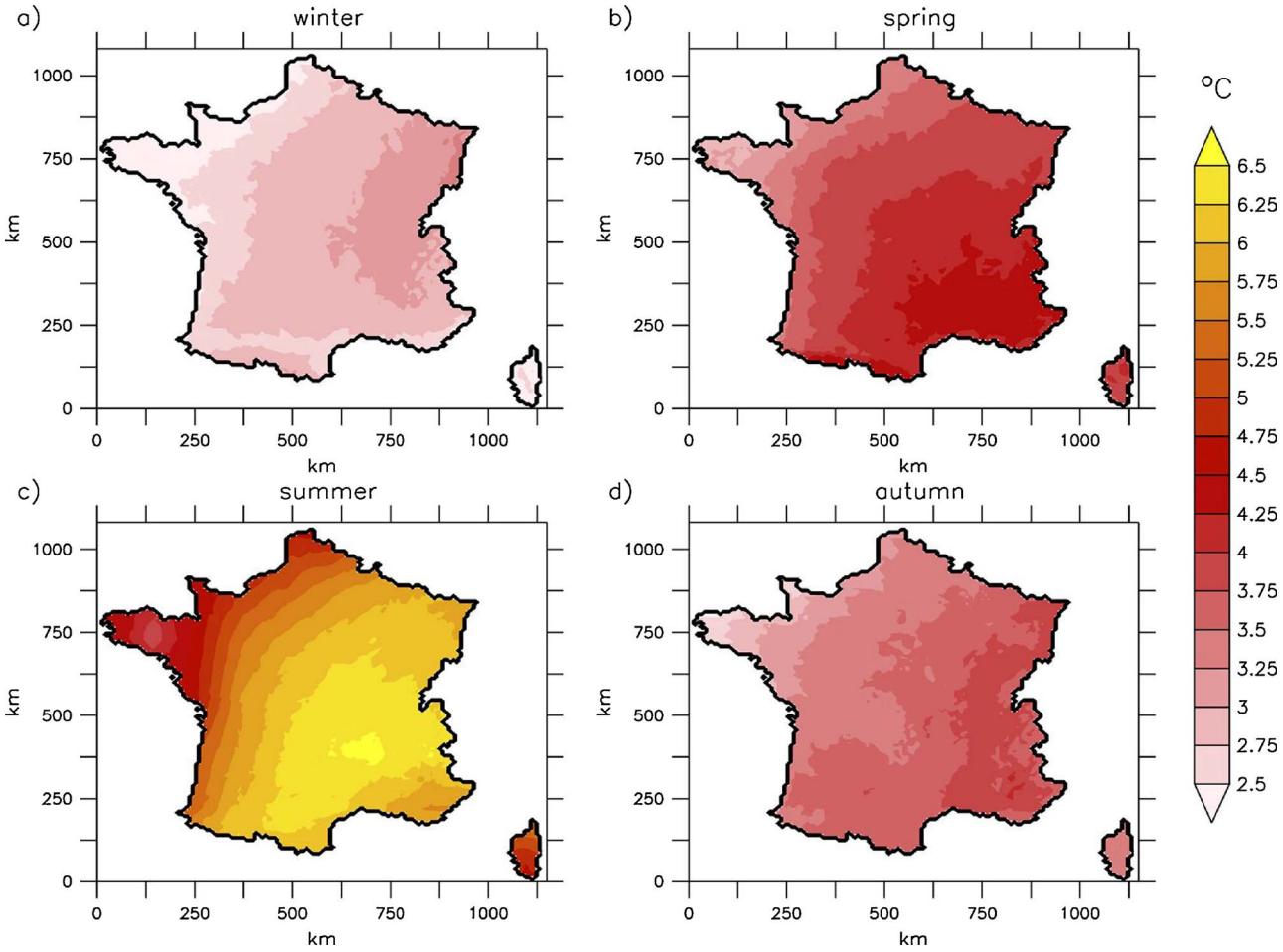

Fig. 3. Climate model ensemble mean of the seasonal anomalies of the surface air temperature (in °C) over the last 30-year of the 21st century (2071–2100) with respect to the baseline period (1980–2009), for RCP8.5 scenario, for (a) winter; (b) spring; (c) summer; (d) autumn.

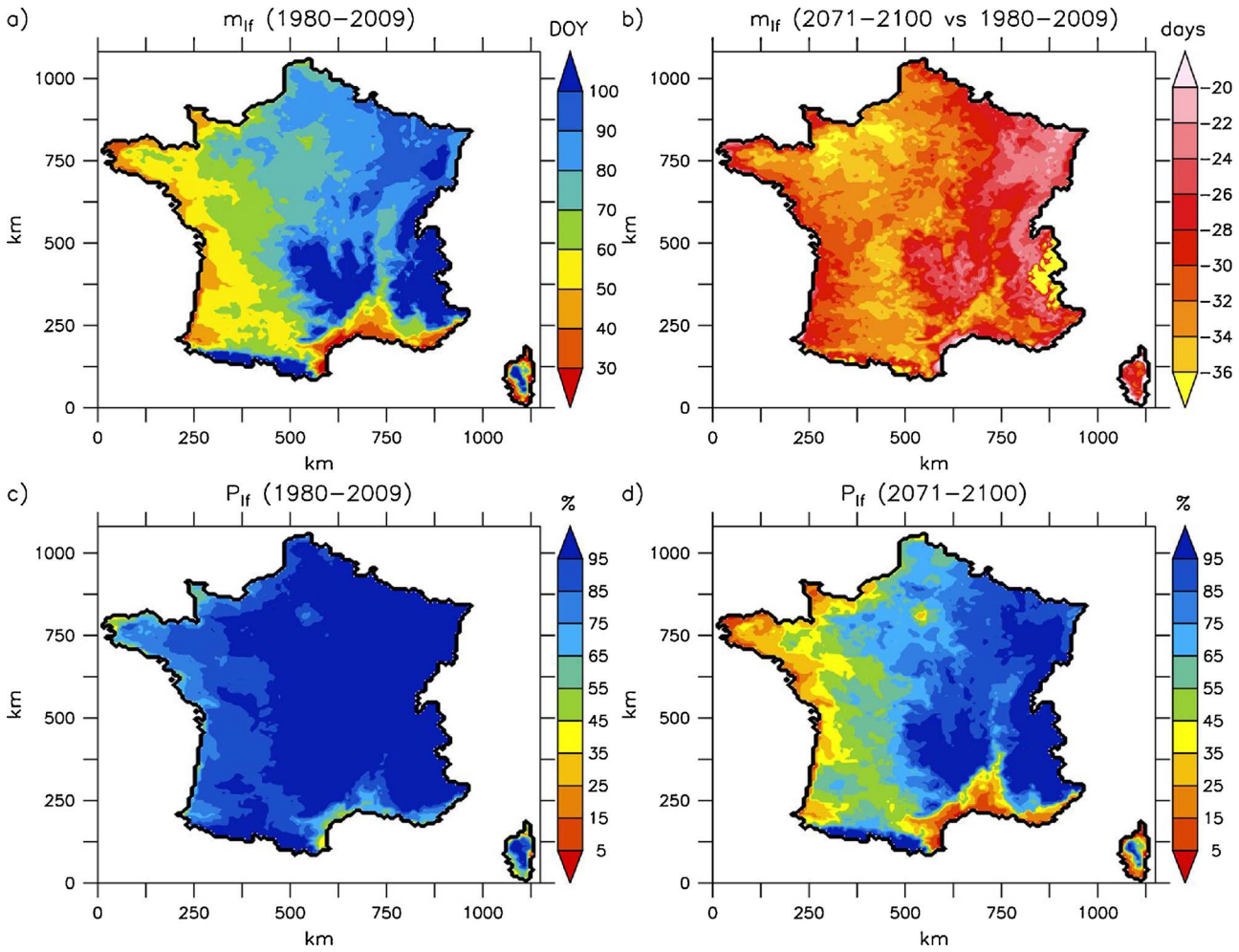

Fig. 4. Occurrence and frequency of the present-day characteristic last frost day of the year and their anomaly at the end of the 21st century. Maps have been calculated by averaging the results of the 8 climate models under RCP8.5 emission scenario. (a) Mean last frost day (m_{lf}, in *DOY)* for the baseline period (1980–2009); (b) Anomaly of m_{lf} (in days) between the 30-year period at the end of the RCP8.5 simulation (2071–2100) with respect to the baseline period (1980–2009). (c) Percentage (in%) of years encountering at least one day satisfying the conditions of frost (P_{lf}), *i.e.* Tavg $< 2\,^{\circ}C$, and Tmin $< -2\,^{\circ}C$, over the baseline period (1980–2009). (d) Anomaly (in%) in P_{lf} between the 30-year period at the end of the RCP8.5 simulation (2071–2100) and the baseline period (1980–2009). Results take into account the ensemble mean of the climate model simulations.

account for the possibility of the lack of frost days over a single year.

The occurrence of at least one frost day over a single year appears to have a 100% probability for the period 1980–2009 over most of the France. The only exceptions are represented by the coastal regions, where on average it occurs for around 50–60% of the years in the Mediterranean region and for around 75–85% of the years in the Atlantic sector (Fig. 4c). Future projections show that years without frost events become more frequent all over the France (Fig. 4d). The most significant changes involve the coastal regions. Projected frost days become a very rare event in the Mediterranean sector, where less than 20% of the years counts at least one frost day at the end of the 21st century. A strong decrease in frost days is also evidenced in the Atlantic sector, with around 50% of the years showing at least one frost day at the end of the 21st century. In the continental regions, although they show the strongest increase in mean temperature, the occurrence of frost days over a year is not precluded at the end of the 21st century, with around 90% of the years still experiencing at least one frost day over Alsace, Burgundy and Champagne.

4.3. Budburst in future projections

In Fig. 5 we show the characteristic budburst m_{bb} dates over France for present-day conditions (1980–2009) and their anomalies Δm_{bb} at the end of the 21st century (2071–2100) for the three phenological models considered in this study. These maps accounts for the ensemble mean of the 8 climate models. Here, we only displayed results for the Chardonnay that were available for the three different models (see Supplementary Figs. 1 and 2 for a comprehensive view on all the varieties according to GDD_5 and BRIN models), and only accounting for its current suitability for high-quality production (Jones, 2006) to better visualize the significant results.

Phenological models qualitatively agree in simulating the present-day characteristic budburst date m_{bb} (Fig. 5a, c and e). In particular, GDD_5 and BRIN models appear to produce almost identical results. The FENOVITIS model, although simulating an average budburst day over France consistent with that in the other models, tends to underestimate the inter-regional differences, due to its lower sensitivity to differences in temperature.

This overall agreement vanishes in the simulation of the future budburst, with results that strongly differ depending on the budburst model. For the GDD_5 model, the increase in temperature under future climate scenarios translates in an overall anticipation of bud break at the end of the 21st century (Fig. 5b). This could be expected as this phenological model only accounts for the post-dormancy phase, and the budburst is exclusively determined by the temperature forcing. Earlier budburst are more pronounced in those regions featuring an amplified warming trend, *i.e.* Alsace, Burgundy and Champagne, than in the regions experiencing a subdued warming trend, *i.e.* Mediterranean and

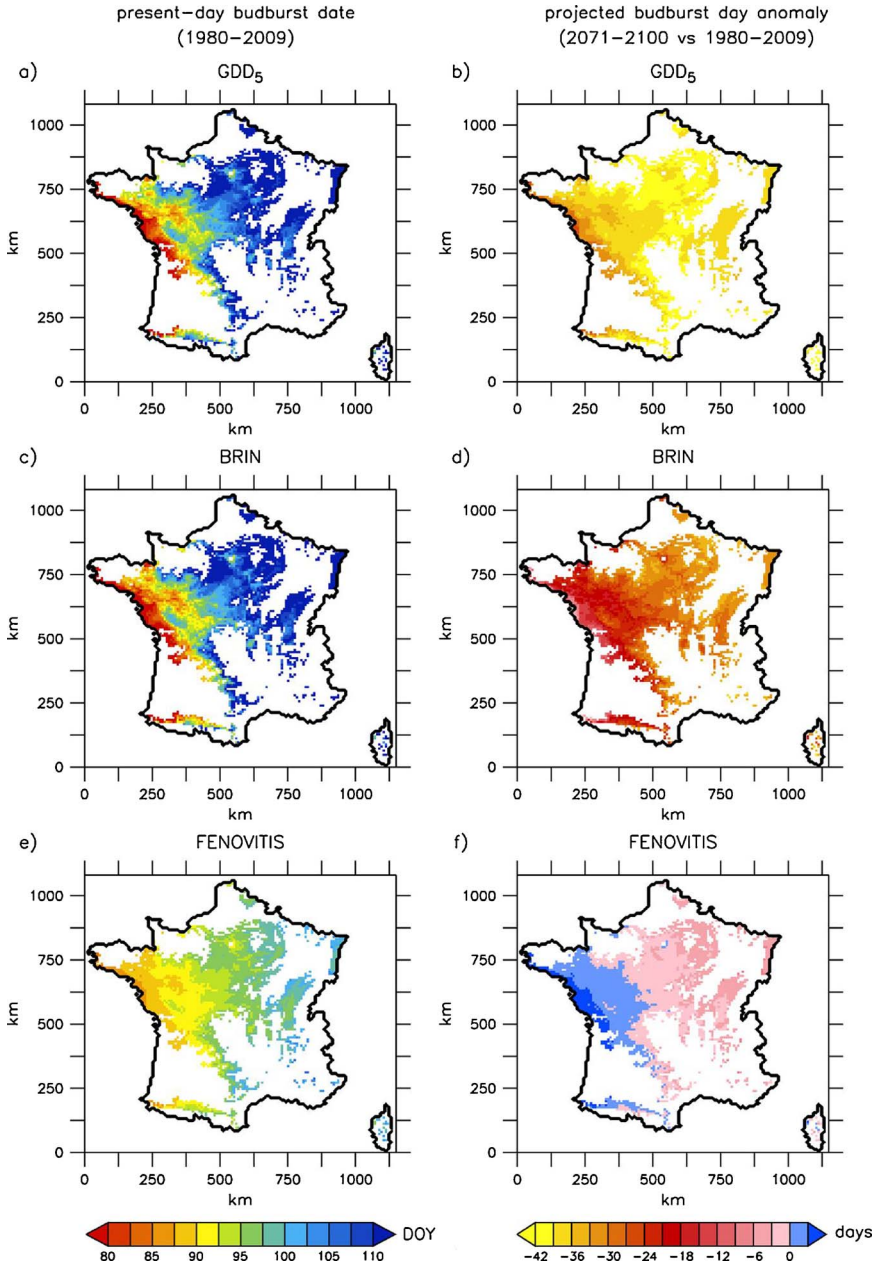

Fig. 5. Pattern of the (a) (c) (e) characteristic budburst day over the year (in DOY) and (b) (d) (f) its anomaly (in days) at the end of the RCP8.5 simulation (2071–2100) with respect to the present-day climate conditions (1980–2009) as simulated by the different phenological models for Chardonnay variety. *Upper panels* indicate results obtained with GDD_5 model, *middle panels* indicate results obtained with BRIN model and *lower panels* indicate results obtained with FENOVITIS model. For a given phenological model, maps display the ensemble mean of the 8 climate model results. Maps only take into account the current suitability regions for high-quality production according with Safran data from 1959 to 2014. Suitable regions for Chardonnay have been here identified as those areas satisfying the classification detailed in Jones (2006) during the historical period.

Atlantic sectors. The BRIN model also exhibits a widespread anticipation of the budburst date at the end of the century (Fig. 5d), which is qualitatively similar to that shown by the GDD_5 model. However, the advance in budburst date is clearly less pronounced than in the GDD_5 model. This is the direct effect of the inclusion of the dormancy period for the BRIN model. Indeed, under warmer climate conditions, such a period tends to increase, thus smoothing the budburst precocity. The FENOVITIS model, contrary to the other two models, simulates a slight advance of budburst date in the continental regions and even a postponement in Atlantic coastal regions (Fig. 5f). This is, again, symptomatic of its lower sensibility to changes in temperature when simulating budburst date, at least for its present calibration.

4.4. The projected risk of tardive frost in France

The different responses of the phenological models in simulating the future budburst days imply different characterization of the risk of tardive frost under warmer conditions. In order to well identify these differences, we first focus on the Chardonnay variety for which budburst simulations were available for the three phenological models. We successively extend such an analysis to all the varieties for GDD_5 and BRIN model, also accounting for the uncertainty of the climate model projections, thus presenting a comprehensive portrait for the French panorama.

4.4.1. Main differences between the phenological models

The risk of tardive frost P_{tf} for both the baseline period (1979–2008) and the period at the end of the 21st century (2071–2100) have been calculated (Eq. (8)) for the ensemble of 8 climate models and displayed for Chardonnay in Fig. 6. For the baseline period, the average risk P_{tf} over France appears to be similar in the three phenological models (Figs. 6a, c, and e). However, at the end of the 21st century we found markedly different responses. For GDD_5 model, the risk of tardive frost P_{tf} increases almost everywhere under warmer climate conditions, notably in the continental region (Fig. 6b). According to the BRIN model, this risk increases in the continental region, while it decreases in the coastal regions (Fig. 6d). On the contrary, FENOVITIS model evidences a decreasing risk all over the France (Fig. 6f).

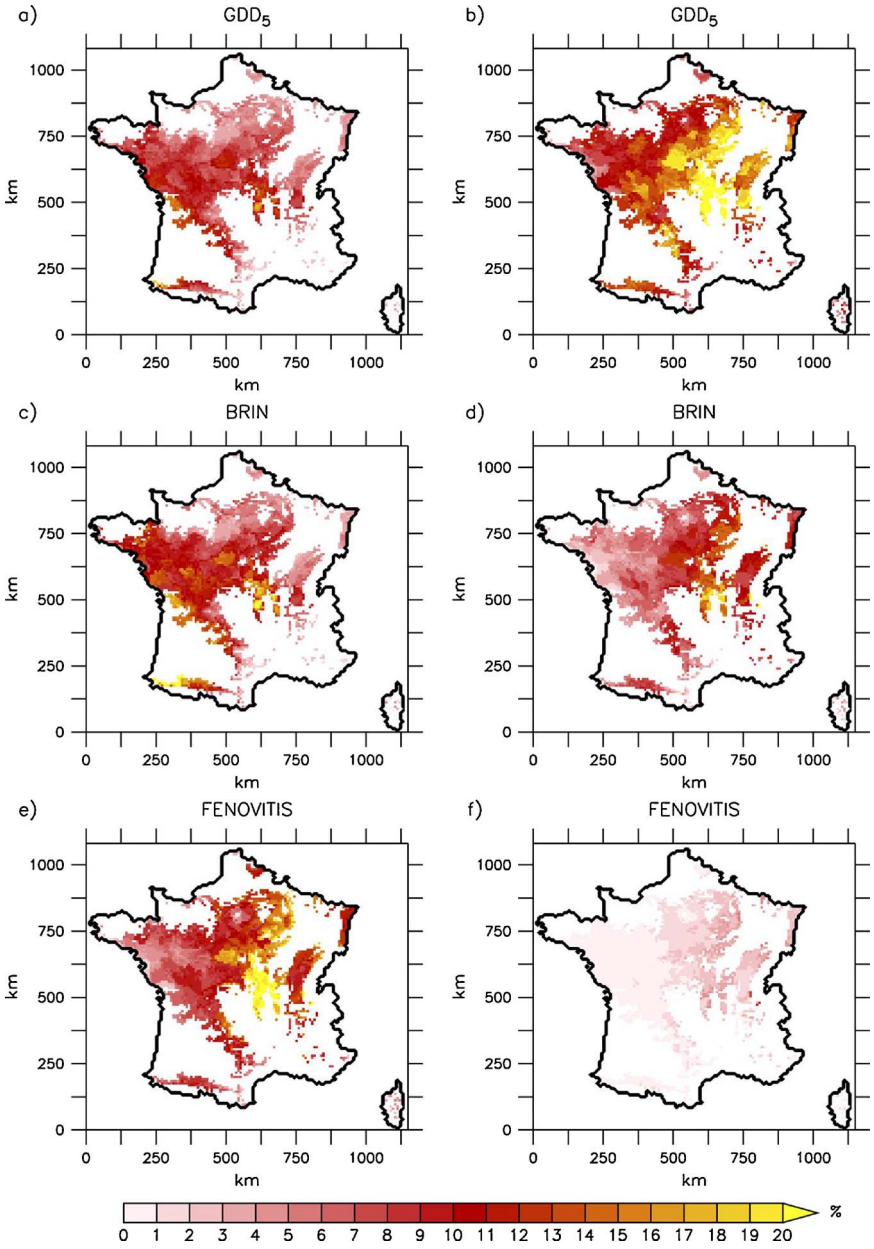

Fig. 6. Pattern of the probability of tardive frost (in%) for Chardonnay variety under (a) (c) (e) present-day climate conditions (1980–2009) and (b) (d) (f) future climate conditions as projected by RCP8.5 simulations for the different phenological models. *Upper panels* indicate results obtained with GDD_5 model, *middle panels* indicate results obtained with BRIN model and *lower panels* indicate results obtained with FENOVITIS model. Results concern the ensemble mean of the 8 climate models. Maps only take into account the current suitability regions for high-quality production according with Safran data from 1959 to 2014. Suitable regions for Chardonnay have been here identified as those areas satisfying the classification detailed in Jones (2006) during the historical period.

These different responses can be interpreted in Fig. 7d, where the main statistical features characterizing the different modeled distributions of budburst dates p_{bb} for Chardonnay in Champagne region have been compared with the main statistical features characterizing the occurrence of the last frost day p_{lf}. For the baseline period, the GDD_5 and BRIN models simulate a very similar characteristic budburst (respectively 29th and 30th of April), while FENOVITIS model reproduces the earliest m_{bb} (8th of April). Differences among the budburst models for present-day conditions also involve the interannual variability. On the one hand, the GDD_5 and BRIN models produce budburst dates spanning over a relatively wide range of time (respectively σ_{bb} = 11 days and σ_{bb} = 14 days). On the other hand, the FENOVITIS model reproduces a much less variable budburst date over the years (σ_{bb} = 6 days), thus further suggesting its lower sensibility to temperature changes. Overall, this yields an initial risk of tardive frost P_{tf} for Chardonnay in Champagne that is higher for the FENOVITIS (P_{tf} = 18.1%) model than for the GDD_5 (6.0%) and BRIN (6.1%) models.

The mutual differences concerning the interannual variability also subsist for future climate conditions. Instead, the simulation of the mean budburst date m_{bb} strongly varies between the phenological models over the period 2071–2100. The GDD_5 model shows the strongest changes in m_{bb}, with a mean anticipation of about 40 days over the last 30 years of the century, while according to the BRIN model such anticipation is close to 35 days. Since (*i*) the probability to experience at least one frost day over a year remains close to 100% (Fig. 4d and 7d) and (*ii*) the precocity of the budburst day is more pronounced than that of the last frost day (Figs. Fig. 44b and Fig. 77d), the risk of tardive frost at the end of the century increases for both GDD_5 (P_{tf} = 18.8%) and BRIN (P_{tf} = 15.0%) models. In the FENOVITIS model the characteristic advance in budburst date is only limited to a few days (Fig. 5f and d), *i.e.* less than 5 days, likely due to its low sensitivity to temperature changes, thus producing a drastic decrease of the risk of tardive frost at the end of the 21st century (P_{tf} = 2.9%).

This analysis has been extended to all the varieties considered in this study (Fig. 7), thus allowing a comprehensive risk assessment on tardive frost for grapevine over France (Fig. 8) by accounting for (*i*) the different climatic regions (Fig. 8), (ii) the different phenological models

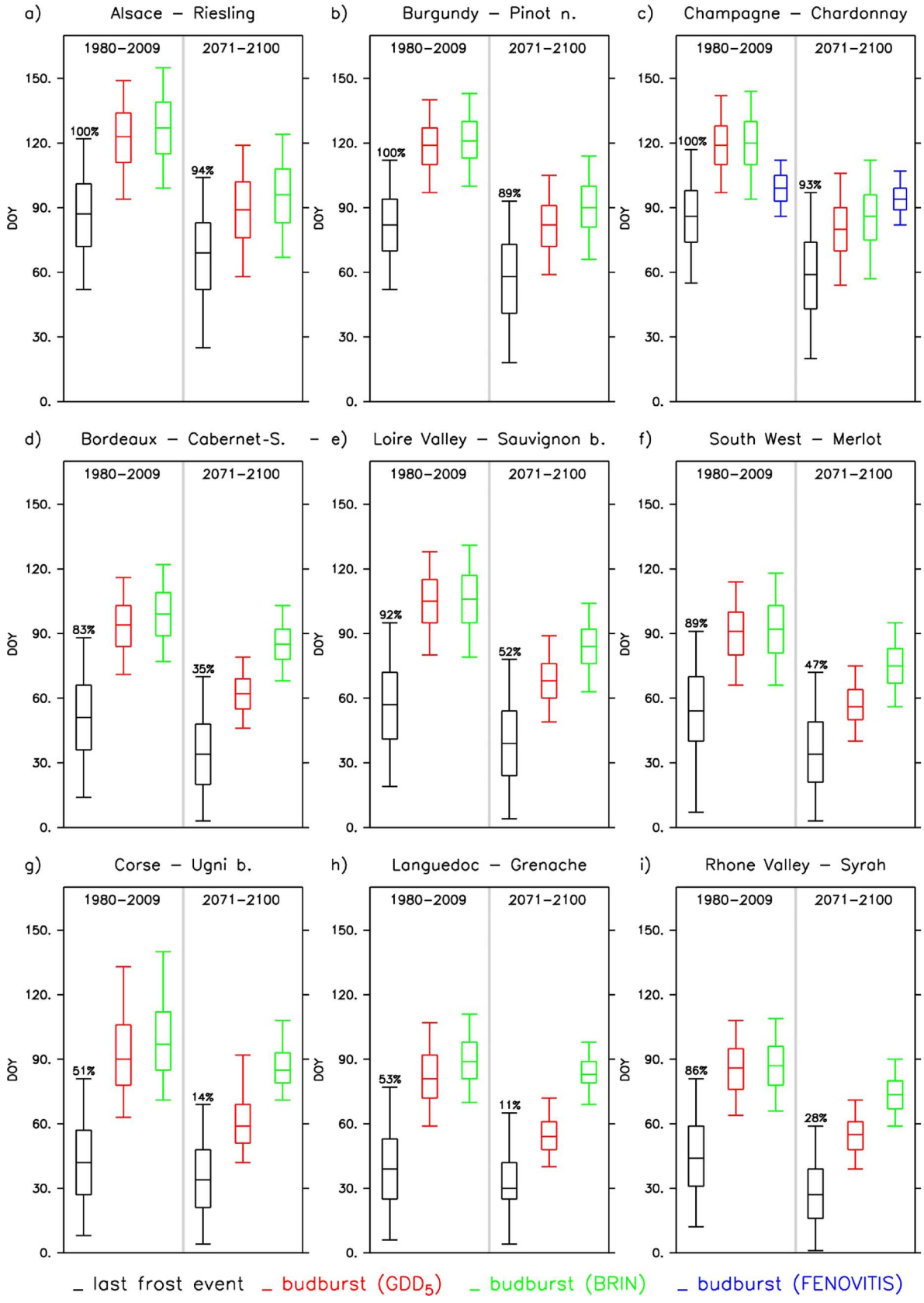

(caption on next page)

Fig. 7. Box-and-whisker plots comparing the distribution of the characteristic last frost day p_{lf} over the year (*black diagrams*), with the distribution of the characteristic budburst date p_{bb} over the year according with GDD_5 model (*red diagrams*) BRIN model (*green diagrams*) and FENOVITIS model (*blue diagrams*). Concerning each phenological model, results are the ensemble mean of the 8 climate model projections for RCP8.5 scenario. In each panel, left side distributions are relative to the period 1980–2009, while right side distributions correspond to the period 2071–2100. The bands inside the boxes indicate the expected values of the mean distributions, the bottom and the top of the box indicate respectively their 25 and 75 percentiles, while whiskers indicate their 5 and 95 percentiles. Values on top of the black diagrams indicate the percentage of years experiencing at least one day satisfying the conditions of frost event during the 30-years, *i.e.* $(N_f/30)*100$. The computation has been performed for a) Riesling in Alsace, b) Pinot Noir in Burgundy, c) Cabernet-Sauvignon in Bordeaux, d) Chardonnay in Champagne, e) Ugni blanc in Corse, f) Grenache in Languedoc, g) Sauvignon blanc in Loire Valley, h) Syrah in Rhone Valley and i) Merlot in South-West. (For interpretation of the references to colour in this figure legend, the reader is referred to the web version of this article.)

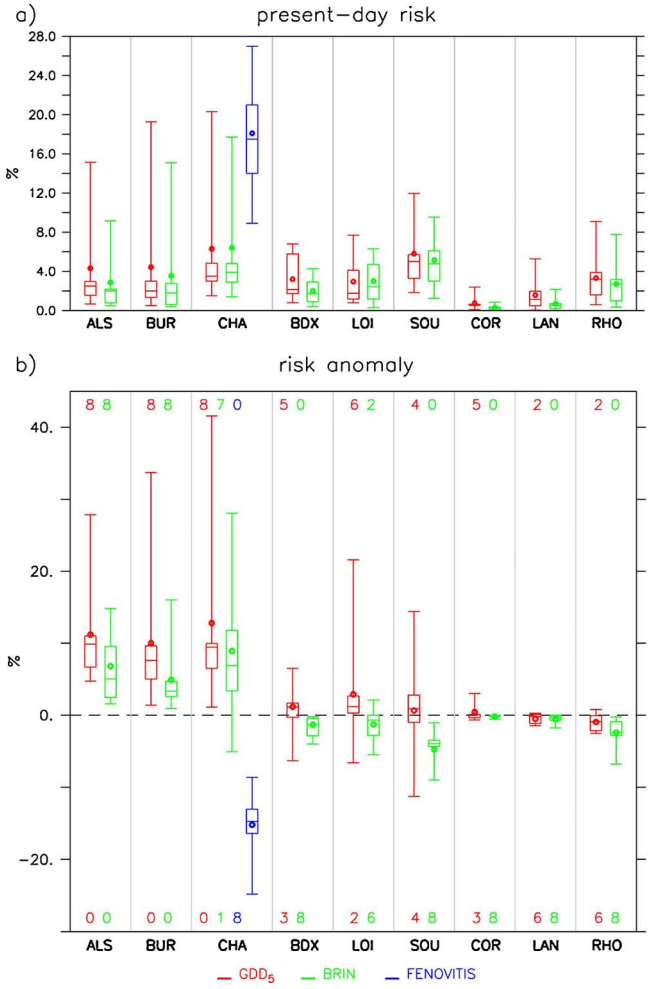

Fig. 8. Box-and-whisker plots showing the distribution of the projected probability of tardive frost P_{tf} (%) among the 8 climate models. The probability of tardive frost has been calculated in the nine checkpoints and according with the different budburst simulations, *i.e.* GDD_5 model (*red diagrams*), BRIN model (*green diagrams*) and FENOVITIS model (*blue diagrams*), of their representative varieties. The resulting distributions are related to a) the baseline period (1980–2009) and b) its anomaly at the end of the 21st century (2071–2100). The band inside each box indicate the median of P_{tf} among the different climate model results, while the bottom and the top of each box indicate respectively their 25 and 75 percentiles. Whiskers coincide with the minimum and the maximum among the 8 different climate model results, while circles indicate their mean. The values on the top (bottom) of the lower panel indicate the number of climate models exhibiting an increasing (decreasing) risk P_{tf}. (For interpretation of the references to colour in this figure legend, the reader is referred to the web version of this article.)

and (*iii*) the uncertainty associated with the different climate models (Fig. 8). In order to present a schematic view on the wide range of possible scenarios, in Figs. 7 and 8 we assigned to each checkpoint a representative variety (see also maps in Supplementary Figs. 3 and 4 for a comprehensive risk anomaly pattern associated with each variety according to GDD_5 and BRIN models). The non-homogeneous increase in temperature for future projections, along with the different growing requirements of the grapevine varieties, differentiates the evolution of the risk of tardive frost. Depending on the specific budburst model, we found markedly diverse responses between continental region, oceanic region and Mediterranean region. These results do not qualitatively change if a different definition of frost day, *i.e.* t_f such that $T_{min} < 0\,^{\circ}C$, is used (Supplementary Figs. 5 and 6).

4.4.2. Risk exposure in continental regions (Alsace, Burgundy and Champagne)

The continental region appears to be the most vulnerable, where typical varieties are already the most exposed to tardive frosts for present-day conditions. If we consider the climate models ensemble mean and spread, the probability of tardive frost P_{tf} in 1980–2009 spans from 2.9 ± 3.0% for Riesling in Alsace according with BRIN model to 18.1 ± 6.6% for Chardonnay in Champagne according with FENOVITIS model (Fig. 8a).

Beyond the exception of the Chardonnay in FENOVITIS model already illustrated, the risk of tardive frost in the continental regions appears to strongly increase throughout the 21st century. In Alsace, the risk for Riesling may even be tripled with respect to the baseline period, *i.e.* $\Delta P_{tf} = 11.2 \pm 7.4\%$ in GDD_5 model and $\Delta P_{tf} = 6.8 \pm 5.3\%$ in BRIN model (Fig. 8b). The same is also valid for Pinot noir in Burgundy, *i.e.* $\Delta P_{tf} = 10.1 \pm 9.9\%$ in GDD_5 model and $\Delta P_{tf} = 5.0 \pm 4.7\%$ in BRIN model, and, as already mentioned, for Chardonnay in Champagne, *i.e.* $\Delta P_{tf} = 12.8 \pm 11.9\%$ in GDD_5 model and $\Delta P_{tf} = 8.9 \pm 10.0\%$ in BRIN model. Such a common response is due to the strong warming trend projected over the continental regions (Fig. 3), which causes the major advance of budburst date for the local grapevine varieties (Fig. 7a, c, and d). At the same time, the occurrence of the last frost day also anticipates but more moderately than the budburst. These differential responses increase the possibility to expose already broken buds to frost conditions.

Fig. 8 also allows visualizing the spread deriving from the climate models and its distribution. For a specific region and given a specific phenological model, there exists a large (qualitative) consensus among the climate models in simulating the anomaly of the risk of tardive frost. For instance, all the 8 climate models project an increasing risk for Pinot noir in Burgundy when GDD_5 model is considered. However, the uncertainty remains large, with this anomaly spanning from $\Delta P_{tf} = +5.03\%$ according to bcc-csm1-1-m model, to $\Delta P_{tf} = +33.73\%$ according to BNU-ESM model. These features, *i.e.* inter-climate model qualitative agreement but large uncertainty, are generally valid for all the varieties characterizing the continental region (Fig. 8).

4.4.3. Risk exposure in Atlantic regions (Bordeaux, Loire Valley and South-west)

In the Atlantic sector, the probability of tardive frosts for its local typical cultivars appears to be generally more moderate than that in the continental regions due to the proximity of the ocean. For instance, according to the GDD_5 model, the risk of tardive frost for the baseline period spans from 2.1 ± 1.7% for Cabernet-Sauvignon in the western part (*e.g.* Bordeaux region) to 5.8 ± 5.0% for Sauvignon blanc in the most interior part (*e.g.* South-West region).

For the future, this risk results, on average, rather stable. For the GDD_5 model the risk of tardive frost at the end of the 21st century will be unaltered or slightly higher, *i.e.* from $\Delta P_{tf} = +0.2 \pm 3.9\%$ in Bordeaux to $\Delta P_{tf} = +2.9 \pm 8.1\%$ in Loire Valley. Instead, simulations with BRIN model show a general slight-to-moderate decrease of this risk, *i.e.* from $\Delta P_{tf} = -1.3 \pm 2.4\%$ in Loire Valley to

$\Delta P_{tf} = -4.0 \pm 2.5\%$ in South-West region.

These moderate changes are determined by the influence of the ocean, which locally mitigates the effects of global warming. The dates of budburst are projected to generally advance more than the last frost days (Fig. 7b, g, and i) thus incrementing the possibility of late frost. However, years featuring at least one frost day in the future are not routinely met (Fig. 4d), thus limiting the occurrence of possible tardive frost events. These contrasting factors ultimately produce limited changes in the future probability of tardive frost events in the Atlantic sector.

The qualitative model consensus subsists when considering BRIN model, while climate model uncertainty increases when considering GDD_5 model. However, inter-climate model spread appears to be generally lower than for continental regions (Fig. 8).

4.4.4. Risk exposure in Mediterranean regions (Corse, Languedoc and Rhone Valley)

In the region overlooking the Mediterranean Sea, the present-day risk of tardive chill for typical local cultivars is relatively low due to the mild climate characterizing this region, *i.e.* from 0.3 ± 0.2% for Ugni blanc in Corse according to BRIN model to 3.3 ± 2.7% for Syrah in Rhone Valley according to GDD_5 model (Fig. 8a). For future projections, this risk appears to remain relatively low, and is even cancelled out in some areas. This is mainly a direct consequence of the strong decrease in years experiencing at least one frost day, which implicitly precludes the occurrence of tardive chill. Near the Mediterranean coast, the probability to experience at least one day satisfying the conditions of frost becomes around 10% at the end of the 21st century (Fig. 4d). Such a probability slightly increases by moving away from the coasts, *e.g.* towards the Rhone Valley, but it is not effective in determining a significant increase in late frost events despite the advance in the budburst date at the end of the 21st century projected over this region (Fig. 7e, f, and h). In general, independently of the phenological model, climate models agree in the projection of the already low risk of tardive frost to decrease at the end of the 21st century over the whole Mediterranean sector.

5. Discussion

The analysis of the risk of tardive frost for French grapevine varieties under future climate conditions gives contrasting results. The GDD_5 model shows an increasing risk over a large part of France, while according to FENOVITIS model this risk will decrease everywhere in France. In between these two opposite projections, the BRIN model simulates an increasing risk in the continental regions of France and a decreasing risk in the regions bordering the Atlantic Ocean and Mediterranean Sea. Such divergent results are primarily determined by the uncertainty between the different phenological models, while climate models qualitatively agree in simulating these different patterns once the method for the budburst calculation is fixed. Nevertheless, results evidence a wide inter-climate models spread, thus also implying a large uncertainty in determining the extent of an increasing or a decreasing risk of tardive frost over a certain region. An important caveat in this context is that such an uncertainty may be even underestimated due to the fact that only 8 climate models have been used in this study. This choice was related with data availability at the daily frequency, but up to 40 models are available in the CMIP5 for lower output frequency. By using this full-set of 40 CMIP5 models, Sgubin et al. (2017) found that the northern North Atlantic is the region with the largest uncertainty in temperature projections over the Northern Hemisphere. Depending on their response in the subpolar gyre, models were clustered in 3 main typologies, that typify different temperature evolution over the western Europe. Since the 8 models used in this study belong to the same cluster, *i.e.* non-abrupt models, the uncertainty deriving from climate models would possibly be higher if models belonging to other clusters could have been considered.

The main differences between the phenological models stem from their different operations of the dormancy and post-dormancy submodels and how they simulate the lengths of chill state and forcing state (Fig. A1). The dormancy period likely represents the most delicate phase in the implementation of the budburst model. In general, the parameterization of a phenological model is based on the simultaneous observations of phenological stages' achievement and *in situ* temperature time series. While budburst is easily observable on field, endodormancy induction and break are not, although they can be observed in laboratory using specific experiments (Chuine, 2016). This represents the biggest limit of such an approach, as it is not possible to estimate the actual days starting from which the chill state and the forcing state are active. As a consequence, phenological models make different assumptions for the dormancy sub-model, which ultimately determine the different responses of the budburst models to warmer-than-present climate conditions.

While these three phenological models perform well when simulating the budburst dates for present-day climate conditions, no assessment about their reliability can be made concerning their performance for future climate. At the current stage of knowledge, their applicability in the context of climate change is uncertain and it is not possible to establish which, among them, produce the most plausible reproduction of budburst dates under warmer conditions. The fact that their results significantly diverge for future climate projections discloses the urgent need to test their validity beyond the present-day climate conditions.

Nevertheless, our results evidence some peculiarities of the FENOVITIS model that may be interpreted as intrinsic bias. The spring temperature over the Champagne region is projected to increase by 4 °C within the end of the 21st century for RCP8.5 scenario. According to the FENOVITIS model, this would produce an advance of around 5 days in the characteristic budburst day. Such a ratio appears to be underestimated if historical data are considered. Indeed, by analyzing observed budburst dates and temperature time series over Tuscany, Orlandini et al. (2009) found that in the period 1955–2007 the increase of 0.9 °C in annual mean temperature was associated with a statistically significant anticipation of 16 days in the budburst date. Moreover, temperature observations over the Bordeaux region show an increase of about 1 °C over the last 50 years of the 20th century. In the same time, measures over this region show that the date of the observation of the first bud reaching the stage "green tip" prior to 1980s was around the 24th of March, while this characteristic date oscillates around the 11th of March after the 1993 (Bois, 2007).

These observations suggest that the anticipation of budburst date may actually be more sensitive to temperature changes than what the FENOVITIS model show for future projections. This represents an important caveat, since previous studies carried out by using FENOVITIS-like budburst models have always prefigured a decreasing risk of late frost exposure for future climate conditions (Molitor et al., 2014; Mosedale et al., 2015). Yet, the intrinsic bias that likely affects FENOVITIS model (at least for its present configuration) hints at the possibility that such a risk might be underrated.

6. Conclusions

The present study presents the first comprehensive analysis of the risk of future late frost damage for viticulture over France, where wine production represents a crucial sector for both economy and culture. Although episodes of extremely cold days tend to decrease both in frequency and severity throughout the 21st century according to the 8 climate models, our results show that the risk of tardive frosts may possibly increase in the future. This apparent contradiction stems from the fact that, over certain regions, the anticipation of the bud break is projected to be more pronounced than the precocity of the last frost event. For early maturity varieties in continental regions, this risk significantly increases when GDD_5 or BRIN model are used for the

simulation of the budburst day, while FENOVITIS model shows a decreasing trend at the end of the 21st century. For the Atlantic and Mediterranean regions, only GDD_5 show a slight increase of such a risk, while BRIN and FENOVITIS models prefigure a near negligible risk for the future. Which budburst model is the most reliable for future climate scenarios remains an open question and likely discloses one of the main challenge for the scientific research in the viticulture field, that is to test the actual validity of the state-of-the-art phenological models under warmer temperature conditions. A preliminary test suggests that GDD_5 and BRIN model produce more plausible results when they are compared with observations over the last 60 years, while the FENOVITIS model tends to underestimate the effects of temperature changes on budburst advance. We therefore urge coming studies to evaluate the applicability of the specific phenological model to future climate conditions, for instance through field experiments forced by artificial source of warming. Nonetheless, our findings may promote preventative interventions in the identified most critical regions of France, where replantation with different plant material (rootstocks and varieties) and/or methods that could reliably delay budburst like postponed pruning (van Leeuwen and Darriet, 2016; van Leeuwen and Destrac, 2017) will likely become necessary to successfully face the on-going climate change.

Acknowledgments

This study has been carried out with financial support from the Region Aquitaine and from the French National Research Agency (ANR) in the frame of the Investments for the future Programme, within the Cluster of Excellence COTE (ANR-10-LABX-45). The storage and the analysis of data have been possible thanks to the cluster CICLAD (Calcul Intensif pour le Climat, l'Atmosphère et la Dynamique) included in the IPSL mesocenter facilities supported by CNRS, UPMC and Labex L-IPSL, which are funded by the ANR (grant number: ANR-10-LABX-0018) and by the European FP7 IS-ENES2 project (grant number: 312979). We are profoundly grateful to Serge Delrot (Université de Bordeaux) and Benjamin Bois (Université de Bourgogne) for having fed constructive discussions around our work. We finally thank two anonymous reviewers for their valuable comments that improved the manuscript.

Appendix A

7.1 The parameterization of the phenological models

The GDD model is most widely used thermal time model for grapevine phenology based on the cumulative heat requirement (Bonhomme, 2000). This model accounts only for the forcing (post-dormancy) period, meaning that the day of endodormancy break is fixed *a priori*. According to this

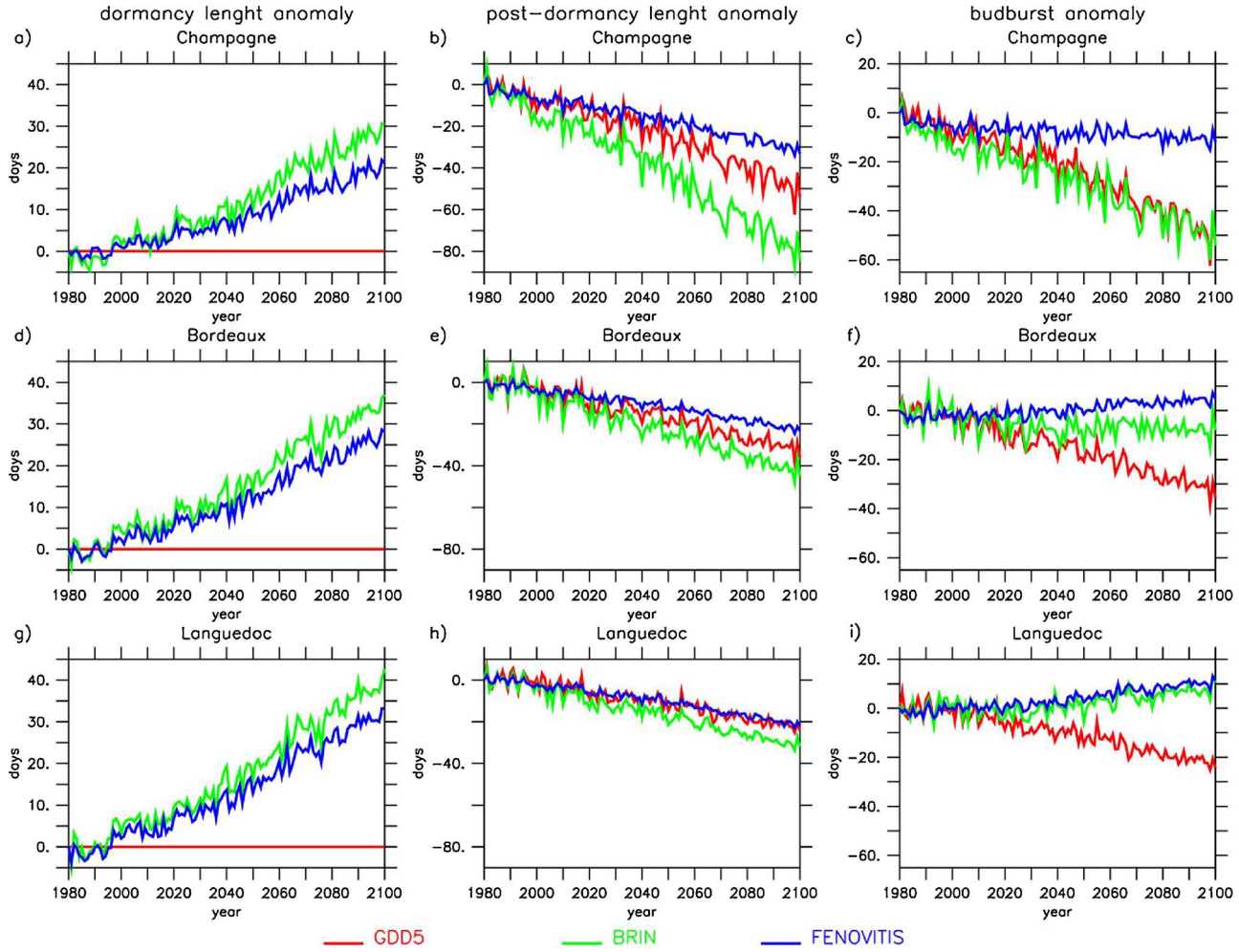

Fig. A1. Time series of the anomalies (in days) of the climate model ensemble mean a) d) g) dormancy period length, b) e) h) post-dormancy period length and c) f) i) budburst date for Chardonnay variety. Results concern the Champagne region (*upper panels*), Bordeaux region (*middle panels*) and Languedoc region (*lower panels*), for RCP8.5 projections. Anomalies are calculated with respect to the corresponding values in 1980. *Red lines* indicate results obtained with GDD_5 model, *green lines* indicate results obtained with BRIN model and *blue lines* indicate results obtained with FENOVITIS model. (For interpretation of the references to colour in this figure legend, the reader is referred to the web version of this article.)

approach, by setting t_{db} as an initial condition of the model (the starting day of the sum), the budburst day t_{bb} takes place once the Eq. (2) is satisfied, where:

$$F_u = \mathrm{GDD}_{T_b} = \begin{cases} 0 \text{ if} T_{\mathrm{avg}} \le T_b \\ T_{\mathrm{avg}} - T_b \text{ if} T_{avg} > T_b \end{cases} \tag{A1}$$

with T_{avg} the mean daily temperature and T_b a base temperature assumed constant. The forcing unit F_u is therefore a linear growing function of the mean temperature T_{avg} when this latter is greater than T_b. Here, we proposed the GDD_5 configuration validated by Garcia de Cortazar-Atauri et al. (2009), for which t_{db} = 1st of January, T_b = 5 °C, while the values of F_{crit} are summarized in Table A1 for the different varieties.

Table A1
Configuration of the different budburst models for present-day climate conditions. Parameters for GDD_5 and BRIN models are those obtained by Garcia de Cortazar-Atauri et al. (2009), while parameters for FENOVITIS model for Chardonnay variety are those calculated in Caffarra and Eccel (2010).

Cepage	GDD_5	BRIN		FENOVITIS		
	F_c	C_c	F_c	C_c	α	β
Cabernet Sauvignon	318.6	106.8	9169.4	/	/	/
Chardonnay	220.1	101.2	6576.7	79	176.26	−0.015
Grenache	321.3	102.2	9174.3	/	/	/
Merlot	265.3	105.7	7595.5	/	/	/
Pinot Noir	258.4	103.6	7468.9	/	/	/
Riesling	257.7	108.2	7471.3	/	/	/
Sauvignon Blanc	294.4	103.9	8352.8	/	/	/
Syrah	265.3	99.2	7818.6	/	/	/
Ugni Blanc	284.7	94.3	9145.4	/	/	/

Since the onset of temperature sum accumulation takes place on a fixed calendar date, the GDD_5 model may neglect the year-to-year variability associated with the dormancy break. However, at least under current climatic conditions, calculating the dormancy period has been shown to be not significant for the accuracy of the bud break timing of the varieties cultivated in France (Garcia de Cortazar-Atauri et al., 2009). Nevertheless, this is not necessarily valid for future climate change, when the likely longer chilling period needed for the achievement of the dormancy break may have a substantial impact in determining the budburst date (Webb et al., 2007; Caffarra and Eccel, 2011; Mosedale et al., 2015).

The BRIN model (Garcia de Cortazar-Atauri et al., 2009) is a sequential model that consists in both a dormancy sub-model and a post-dormancy sub-model, so that the end of the endodormancy is not an initial arbitrary condition as in the GDD model. For the BRIN model, the day of dormancy break t_{db} takes place once the critical threshold of chilling forcing C_{crit} has been reached according to Eq. (1), where the chilling unit C_u is based on the Q_{10} Bidabe's formula (Bidabe, 1965):

$$C_u = Q_{10}^{\frac{-T_{\max}}{10}} + Q_{10}^{\frac{-T_{\min}}{10}} \tag{A2}$$

with T_{min} and T_{max} respectively the minimal and the maximal daily temperatures. Once calculated t_{db}, the forcing state in the post-dormancy period is based on the approximation of the growing degree hours (GDH) cumulated over a day, so that the forcing unit F_u in Eq. (2) is:

$$F_u = \sum_{h=1}^{24} \mathrm{GDH}_{T_b} \approx \begin{cases} 0 \text{ if} \frac{T_{\max}+T_{\min}}{2} \le T_b \\ \frac{T_{\max}+T_{\min}}{2} - T_b \text{ if } T_b < \frac{T_{\max}+T_{\min}}{2} < T_B \\ T_B - T_b \text{ if} \frac{T_{\max}+T_{\min}}{2} \ge T_B \end{cases} \tag{A3}$$

where T_B is the upper base temperature beyond which development rate becomes constant (Moncur et al., 1989). The forcing unit therefore has a linear response to temperature limited by the base parameters T_b and T_B. Here, we used the configuration of the BRIN model proposed by Garcia de Cortazar-Atauri et al. (2009), for which t_0 = 1st of August, Q_{10} = 2.17, T_b = 5 °C and T_B = 25 °C, while the values of C_{crit} and F_{crit} for the different varieties are summarized in Table A1.

The FENOVITIS model is a parallel budburst model consisting in a set of equations describing both dormancy and post-dormancy periods, in which the rate of bud development is related to both the ambient temperature and the stage of chilling (Chuine, 2000). It was originally developed as a simplified version of the UNIFIED model (Chuine, 2000), which provides a general framework for phenological model by gathering in one unique standardized formulation the budburst process of the perennial species. In the dormancy sub-model, the cold action in Eq. (1) is represented by a bell-shape curve defined by two parameters a and c:

$$C_u = \frac{2}{1 + e^{a(T_{\mathrm{avg}}-c)^2}} \tag{A4}$$

The accumulation of forcing units of Eq. (2) is described by the sigmoidal function:

$$F_u = \frac{1}{1 + e^{-0.26(T_{\mathrm{avg}}-16.06)}} \tag{A5}$$

Moreover, contrary to the GDD and BRIN models, the forcing requirement F_{crit} of Eq. (2) in the FENOVITIS model is not a constant value but it varies with time t as it depends on the progression of the chilling state:

$$C_s = \sum_{t_0}^{t} C_u \tag{A6}$$

even after the dormancy break. In particular, the critical forcing requirement F_{crit} of Eq. (2) decreases as chilling increases and it is given by:

$$F_{crit} = \alpha e^{\beta C_s} \quad \text{(A7)}$$

where α and β are two input parameters of the model, with $\beta < 0$. Here, we used the configuration for the Chardonnay, whose parameters were validated by Caffarra and Eccel (2010, 2011) for several viticulture regions of the North-East of Italy, *i.e.* t_0 = 1st of September, a = 0.005, c = 2.8, C_{crit} = 78.692, α = 176.26, β = −0.015. This same configuration of the FENOVITIS model was also used to study the frost risk in the south of England, yet with t_0 = 1st of October (Mosedale et al., 2015). Moreover, the FENOVITIS model was at the base of the DORMPHOT model, which also accounts for the photoperiod effect (not considered in our formulation). This model was used for risk assessment of tardive chill for Muller-Thurgau in Luxemburg (Molitor et al., 2014), as well as to study the effects of climate change to others species, *e.g.* birch in Ireland (Caffarra et al., 2014).

Structural similarities and differences between GDD_5, BRIN and FENOVITIS models are detailed in the example illustrated in Fig. A1, where the anomalies in the simulation of the dormancy and post-dormancy periods for Chardonnay in Champagne, Bordeaux and Languedoc regions have been highlighted and related to the eventual budburst date anomalies. For the GDD_5 model, the anomalies in budburst dates are exclusively determined by the post-dormancy sub-model, since the dormancy period is not accounted for. As a result, due to the increasing temperature in climate projections, the length of forcing period reduces, thus provoking a net anticipation of the budurst in each region. For the BRIN model, the effect of dormancy becomes determinant. The increasing temperature during the autumn and spring expands the time requirement for the dormancy break, thus postponing the activation of the forcing period by around 30 days in the Champagne, up to more than 40 days in Languedoc. Yet the BRIN model also reproduces the strongest reductions in the post-dormancy period, thus counterbalancing the effects of longer lasting dormancy periods. As a final result, the budburst significantly advances in Champagne and Bordeaux, where the forcing period reductions definitely overtake the increase in dormancy periods, contrary to what has been evidenced for the Languedoc, where budburst may even be postponed (but the Languedoc characteristic climate lies out of the suitability conditions for quality production of Chardonnay). For the FENOVITIS model, changes in both dormancy and post-dormancy period are clearly more limited. Moreover, in the western part of France, changes in dormancy period appear to be larger than changes in post-dormancy period, thus causing a delay in the budburst date in future projections. On the opposite, for the eastern part of France, the budburst is projected to anticipate, although such an anticipation is limited only to a few days.

7.2 The calculation of the probability of tardive frosts

In Fig.B1 we detailed each step of the calculation of the probability of tardive frost P_{tf} for three different grape varieties in three different locations, *i.e.* Chardonnay in Champagne region (left panels), Cabernet-Sauvignon in Bordeaux region (central panels), and Grenache in Languedoc region (right panels). The example concerns results obtained with GDD_5 model. For the periods 1980–2009 and 2071–2100, we calculated the probability density function of both budburst day (Eq. (3)) and last frost day (Eq. (5)) occurrence for each single climate model, and we calculated their ensemble mean (upper panels). In the middle panels, we displayed P_{lf} whose definition is given in Eq. (6). These are the necessary parameters to calculate p_{tf} (Eq. (7)), which is plotted in the lower panels. The integral of p_{tf} over the year is what ultimately determines P_{tf}, which is finally the value used in our risk assessment.

This example also illustrates well the main differences between the responses in the three locations, favoring a more detailed interpretation of our results. For the modeled current state of climate (1980–2009), the risk of tardive frost for Chardonnay in Champagne is two times higher than the risk for Cabernet-Sauvignon in Bordeaux and three times higher than the risk for Grenache in Languedoc (Fig. B1g, h and i). These risks evolve in different ways.

The Chardonnay in Champagne region evidences the strongest advance of the mean budburst date m_{bb} for future projections (Fig. B1a). It passes from around beginning of April for present-day conditions to around end of February for future climate conditions. The characteristic date of last frost m_{lf} also anticipates, but such anticipation is more moderate than the one projected for budburst, *i.e.* from about end of March to about beginning of March (Fig. B1a). Moreover, the probability to experience at least one frost day over a single year P_{lf} remains always close to 100% throughout the 21st century (Fig. B1d). As a result, the probability of tardive frosts P_{tf} involving Chardonnay in Champagne significantly increases, passing from 6% in 1980–2009 to 19% in 2071–2100 (Fig. 8g).

The future mean budburst date m_{bb} for the Cabernet-Sauvignon in Bordeaux is also projected to advance more than the characteristic last frost day m_{lf}, with the former projected 1 month earlier than present and the latter about 20 days earlier than present (Fig. B1b). The number of frost days will significantly decrease in the future and the percentage of years featuring at least one frost day goes from more than 90% for present-day conditions to less than 40% for future climate conditions (Fig. B1e). These two mechanisms counterbalance each other: the stronger precocity of the budburst with respect to the last frost day occurrence tends to increase the risk of future tardive frosts, while a less frequent occurrence of years featuring frost days tends to decrease such a risk. The overall result is a nearly unaltered P_{tf}, which goes from 3% for the baseline period to around 4% at the end of the 21st century (Fig. 8h).

For Grenache in Languedoc, we also found substantial budburst anticipation at the end of the 21st century, with a characteristic date m_{bb} going from about the end of March for present-day conditions to about the end of February for future climate conditions (Fig. B1c). However, the occurrence of years featuring at least one frost day sensibly reduces in Languedoc, going from about 50% for the baseline period to about 10% for the last 30 years of the 21st century (Fig. B1f). As a result, the already very low probability of tardive frost P_{tf} for present-day conditions (2%) is projected to remain substantially unaltered for future climate conditions (Fig. B1i).

Appendix B. Supplementary data

Supplementary data associated with this article can be found, in the online version, at https://doi.org/10.1016/j.agrformet.2017.12.253.

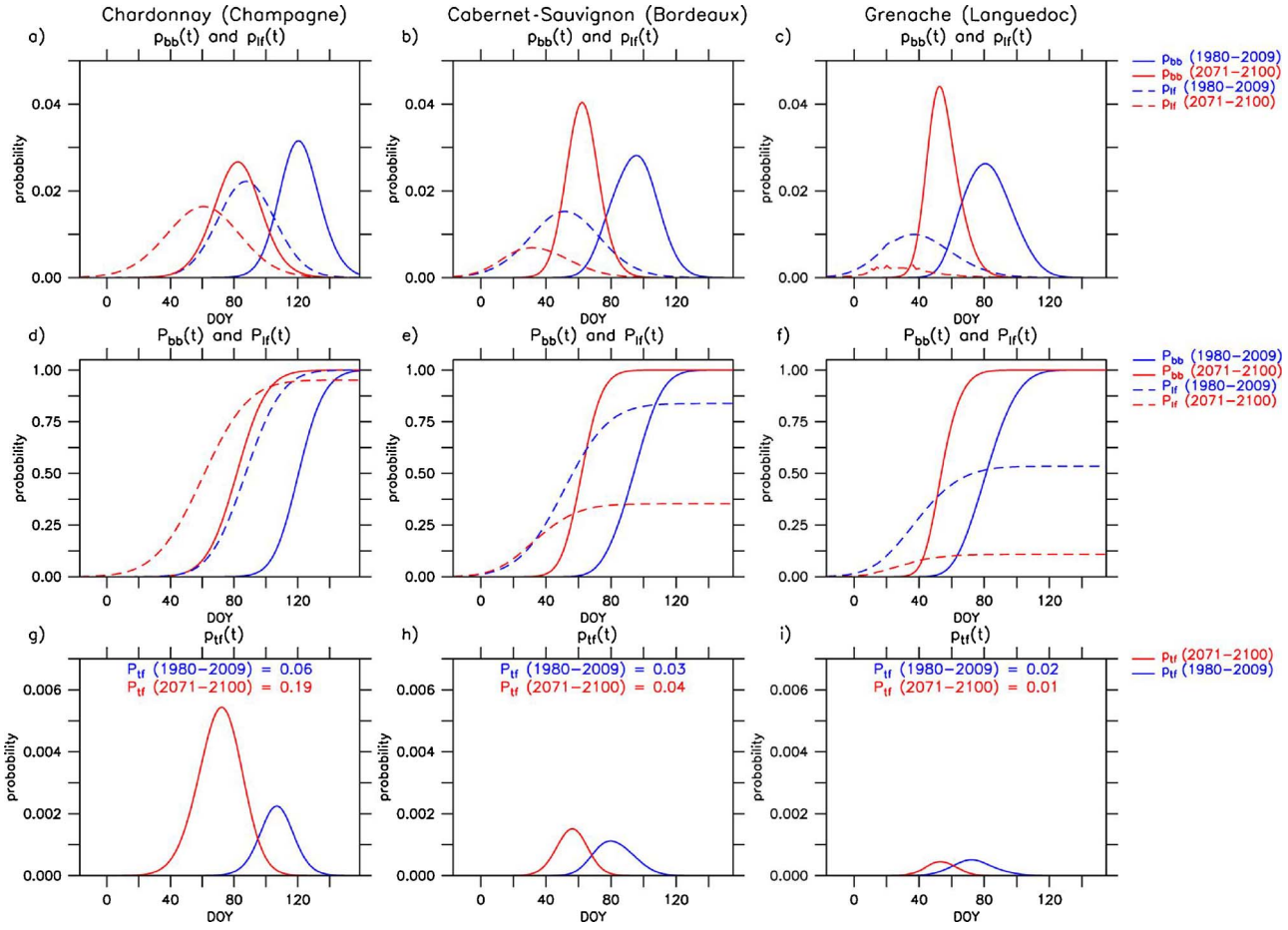

Fig. B1. Example of the step-by-step calculation of the probability of tardive frosts for Grenache in Languedoc (*left panels*), Cabernet Sauvignon in Bordeaux (*central panels*) and Chardonnay in Champagne (*right panels*). Panels *a) b) c)* show the probability density function for the characteristic DOY of the budburst $p_{bb}(t)$ (eq. 3) (*solid lines*) and characteristic DOY of the last frost p_{lf} (eq. 5) (*dashed lines*). Distributions are related to the period 1980–2009 (*blue lines*) and to the period 2071–2100 (*red lines*). Panels *d) e) f)* show their cumulative distribution functions P_{bb} (*solid lines*) and P_{lf} (*dashed lines*) over the 1980–2009 (*blue lines*) and over the 2071–2100 (*red lines*). Panels *g) h) i)* show the probability density function of tardive frost p_{tf} (t) (eq. 7) for the period 1980–2009 (*blue lines*) and the period 2071–2100 (*red lines*). The values of total probability P_{tf} (eq. 8) are also indicated on the top of the panel. Each distribution is relative to the ensemble mean of the 8 climate model results.

References

Bidabe, B., 1965. Contrôle de l'époque de floraison du pommier par une nouvelle conception de l'action de températures. C. R. Acad. Agric. Fr. 49, 934–945.

Bois, B., 2007. Changement climatique et cycle végétatif de la vigne en Gironde: impacts récents et futurs. Actes des 8e journées techniques du Conseil Interprofessionnel des Vins de Bordeaux, Bordeaux, 13 Mars.

Bonhomme, R., 2000. Bases and limits to using degree-day units. Eur. J. Agron. 13, 1–10.

Caffarra, A., Eccel, E., 2010. Increasing the robustness of phenological model for Vitis vinifera cv Chardonnay. Int. J. Biometeorol. 54, 255–267.

Caffarra, A., Eccel, E., 2011. Projecting the impacts of climate change on the phenology of grapevine in a mountain area. Aust. J. Grape Wine Res. 17, 52–61.

Caffarra, A., et al., 2014. Spatial heterogeneity in the timing of birch budburst in response to future climate warming in Ireland. Int. J. Biometeorol. 58, 509–519.

Chuine, I., Kramer, K., Hänninen, H., 2003. Plant development models. In: Schwartz, M.D. (Ed.), Phenology: an Integrative Environmental Science. Kluwer Milwaukee, pp. 217–235.

Chuine, I., 2000. A unified model for budburst of trees. J. Theor. Biol. 207, 337–347.

Chuine, I., et al., 2016. Can phenological models predict tree phenology accurately in the future? The unrevealed hurdle of endodormancy break. Glob. Change Biol. 22, 3444–3460. http://dx.doi.org/10.1111/gcb.13383.

Cuccia, C., et al., 2014. Phenological model performance to warmer conditions: application to Pinot Noir in Burgundy. J. Int. Sci. Vigne Vin 48, 169–178.

Dayon, G., Boe', J., Martin, E., 2015. Transferability in the future climate of a statistical downscaling method for precipitation in France. J. Geophys. Res. Atmos. 120, 1023–1043.

Dee, D.P., et al., 2011. The ERA-iterim reanalysis: configuration and performance of the data assimilation system. Q. J. R. Meteorol. Soc. 137, 553–597.

Duchêne, E., et al., 2010. The challenge of adapting grapevine varieties to climate change. Clim. Res. 41, 193–204.

Fraga, H., Garcia de Cortazar-Atauri, I., Malheiro, A.C., Santos, J.A., 2016. Modelling climate change impacts on viticultural yield, phenology and stress conditions in Europe. Glob. Change Biol. 22, 3774–3788.

Garcia de Cortazar-Atauri, I., Brisson, N., Gaudillere, J.P., 2009. Performance of several models for predicting budburst date of grapevine (*Vitis vinifera* L.). Int. J. Biometeorol. 53, 317–326.

Goodess, C., et al., 2009. Downscaling methods, data and tool for input to impact assessments. ENSEMBLES: Climate Change and its Impacts Summary for Research and Results from ENSEMBLES project. pp. 59–78.

IPCC, 2013. Summary for policymakers. Climate Changes 2103. The Physical Science Basis. Contribution of Working Group I to the Fifth Assessment Report on the Intergovernmental Panel on Climate Change. Cambridge University Press.

Jones, G.V., Davis, R., 2000. Climate influences on grapewine phenology, grape composition, and wine production and quality for Bordeaux, France. Am. J. Enol. Vitic. 51, 249–261.

Jones, G.V., et al., 2005. Climate changes and global wine quality. Clim. Changes 73, 319–343.

Jones, G.V., 2006. Climate and terroir: impacts of climate variability and change on wine. Geosci. Can. Reprint Ser. 9, 1–14.

Lebon, E., 2002. Changements climatiques: quelle consequence pour la viticulture. 6emes Rencontre Rhodaniennes 31–36. Orange, France Institute Rhodanien.

Lorenz, E.N., 1969. Atmospheric predictability as revealed by naturally occurring analogues. J. Atmos. Sci. 26, 636–646.

Maraun, D., et al., 2010. Precipitation downscaling under climate change: recent developments to bridge the gap between dynamical models and the end user. Rev. Geophys. 48, RG3003.

Meinshausen, M., et al., 2011. The RCP greenhouse gas concentrations and their extensions from 1765 to 2300. Clim. Change 109, 213–241.

Mira de Orduña, R., 2010. Climate change associated effects on grape and wine quality and production. Food Res. Int. 43, 1844–1855.

Molitor, D., Junk, J., 2011. Spätfrostschäden 2011–Boten des Klimawandels? Das Deutsche Weinmagazin 22, 30–33.

Molitor, D., et al., 2014. Late frost damage risk for viticulture under future climate conditions: a case study for the Luxembourgish winegrowing region. Aust. J. Grape Wine Res. 20, 160–168.

Moncur, M.W., et al., 1989. Base temperatures for budburst and leaf appearance of

grapevines. Am. J. Enol. Vitic. 40, 21–26.
Mosedale, J.R., Wilson, R.J., Maclean, M.D., 2015. Climate change and crop exposure to adverse weather: changes to frost risk and grapevine flowering conditions. PLoS One 10, e0141218.
Ollat, N., Touzard, J.-M., 2014. Long-term adaptation to climate change in viticulture and enology: the LACCAVE project. Spécial Laccave. J. Int. des Sci. de la Vigne et du Vin 2014, 1–7.
Orlandini, S., et al., 2009. Current trends of agroclimatic indeces applied to grapevine in Tuscany (Central Italy). Q. J. Hungarian Meteorol. Serv. 113, 63–78.
Parker, A., et al., 2011. General phenological model to characterize the timing of flowering and veraison of Vitis vinifera L. Aust. J. Grape Wine Res. 17, 206–216.
Parker, A., et al., 2013. Classification of varieties for their timing of flowering and veraison using a modelling approach: a case study for the grapevine species Vitis vinifera L. Agric. Forest Meteorol. 180, 249–264.
Perry, K.B., 1998. Basics of frost and freeze protection for horticultural grapes. HortTechnology 8, 10–15.
Pieri, P., 2010. Changement climatique et culture de la vigne: l'essentiel des impacts. In: ANR, INRA (Eds.), Changement Climatique, Agriculture et Forêt en France: Simulations d'Impacts sur les Principales Espèces. In: Le Livre Vert du projet CLIMATOR (2007-2010), Ademe editions. pp. 213–223.
Poling, E.B., 2008. Spring cold injury to winegrapes and protection strategies and methods. HortScience 43, 1652–1662.
Quintana-Segui, P., 2008. Analysis of near-surface atmospheric variables: validation of the SAFRAN analysis over France. J. Appl. Meteorol. Climatol. 47, 92–107.
Sarvas, R., 1974. Investigation on the annual cycle of development of forest trees. II. Autumn dormancy and winter dormancy. Commun. Inst. For. Fenn. 84, 1–101.
Sgubin, G., et al., 2017. Abrupt cooling over the North Atlantic in modern climate models. Nat. Commun. 8. http://dx.doi.org/10.1038/ncomms14375.
Trought, M.C.T., Howell, G.S., Cherry, N., 1999. Pratical considerations for reducing frost da in vineyards. Report to New Zealand Winegrowers. New Zealand Winegrowers, Auckland, New Zealand.
Vidal, J.-P., et al., 2010. A 50-year high-resolution atmospheric reanalysis over France with the Safran system. Int. J. Climatol. 30, 1627–1644.
Webb, L.B., Whetton, P.H., Barlow, E.W.R., 2007. Modelled impact of future climate change on the phenology of winegrapes in Australia. Aust. J. Grape Wine Res. 13, 165–175.
Webb, L.B., Whetton, P.H., Barlow, E.W.R., 2011. Observed trends in winegrape maturity in Australia. Glob. Change Biol. 17, 2707–2719.
White, M.A., et al., 2006. Extreme heat reduces and shifts United States premium wine production in the 21st century. Proc. Nat. Acad. Sci. U. S. A. 103, 11217–11222.
Xu, Y., et al., 2012. B. Burgundy regional climate change and its potential impact on grapevines. Clim. Dyn. 39, 1613–1626.
van Leeuwen, C., Darriet, P., 2016. The impact of climate change on viticulture and wine quality. J. Wine Econ. 11, 150–167.
van Leeuwen, C., Destrac, A., 2017. Modified grape composition under climatre change conditions requires adaptations in the vineyard. OENO One 51, 147–154.
van Leeuwen, C., et al., 2008. Heat Requirements for Grapewine Varieties Is Essential Information to Adapt Plant Material in a Changing Climate, 7th International Terroir Congress, 2008-05-19-2008-05-23. pp. 19–2008 Nyon Switzerland.